AD-752 575

STRENGTHENING MECHANISM OF HIGH STRENGTH TITANIUM ALLOYS

Harold Margolin, et al

New York University

Prepared for:

Air Force Materials Laboratory

March 1972

AFML-TR-72-78

STRENGTHENING MECHANISM OF HIGH STRENGTH TITANIUM ALLOYS

H. Margolin
M. A. Greenfield
E. Levine
I. Greenhut
H. Park

New York University
Engineering Research Division

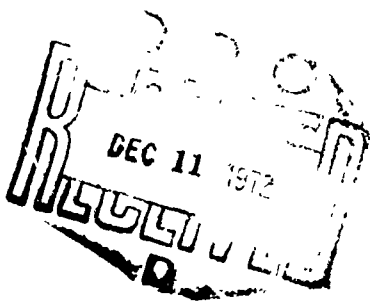

TECHNICAL REPORT AFML-TR-72-78

March 1972

Air Force Materials Laboratory
Air Force Systems Command
Wright-Patterson Air Force Base, Ohio

NOTICE

When Government drawings, specifications, or other data are used for any purpose other than in connection with a definitely related Government procurement operation, the United States Government thereby incurs no responsibility nor any obligation whatsoever, and the fact that the government may have formulated, furnished, or in any way supplied the said drawings, specifications, or other data, is not to be regarded by implication or otherwise as in any manner licensing the holder or any other person or corporation, or conveying any rights or permission to manufacture, use, or sell any patented invention that may in any way be related thereto.

Copies of this report should not be returned unless return is required by security considerations, contractural obligations, or notice on a specific document.

UNCLASSIFIED

Security Classification

DOCUMENT CONTROL DATA - R & D

(Security classification of title, body of abstract and indexing annotation must be entered when the overall report is classified)

1 ORIGINATING ACTIVITY (Corporate author)	2a. REPORT SECURITY CLASSIFICATION
New York University Engineering Research Division New York, N. Y.	Unclassified
	2b. GROUP

3 REPORT TITLE

Strengthening Mechanism of High Strength Titanium Alloys

4 DESCRIPTIVE NOTES (Type of report and inclusive dates)

Summary Technical Report January 1, 1971 - December 31, 1971

5 AUTHOR(S) (First name, middle initial, last name)

Harold Margolin, Ira Greenhut, Michael A. Greenfield, Hoon Park, Ernest Levine

6 REPORT DATE	7a. TOTAL NO OF PAGES	7b. NO. OF REFS
March 1972	~~32~~ 72	6

8a. CONTRACT OR GRANT NO	9a. ORIGINATOR'S REPORT NUMBER(S)
F33615-71-C-1301	
b. PROJECT NO 7351	
c. Task No. 735105	9b. OTHER REPORT NO(S) (Any other numbers that may be assigned this report) AFML-TR-72-78
d.	

10 DISTRIBUTION STATEMENT

Approved for public release; distribution unlimited.

11 SUPPLEMENTARY NOTES	12 SPONSORING MILITARY ACTIVITY
Details of illustrations in this document may be better studied on microfiche.	Air Force Materials Laboratory (LLP) Wright-Patterson Air Force Base, Ohio 45433

13 ABSTRACT

An investigation has been initiated to determine the relationship between the fracture toughness and yield strength in the alpha-beta alloy, Ti-5.25Al-5.5V-0.9Fe-0.5Cu.

Increasing the yield strength of alloy #2 above the 165 Ksi level by warm working to determine the effect on fracture toughness was attempted. No significant increase in yield strength could be achieved by this process. Micrographs show some precipitation of alpha as a result of the working process. A bi-modal grain size was also found in these specimens. It is believed that this is a result of the swaging process.

Specimens heat treated to a yield strength of 185 Ksi have shown a contribution to fracture toughness at lower grain boundary alpha thicknesses than that exhibited in the 165 Ksi yield strength specimens. However, the plateau denoting the maximum contribution to K_Q by grain boundary alpha is reached at nearly the same level as for the 165 Ksi case. A mechanism of dislocation pile-up and stress relief is proposed to explain this behavior.

Vickers hardness tests of both grain boundary and equiaxed alpha increase as the hardness of the matrix increases. Equiaxed alpha is more affected by the matrix hardness than grain boundary alpha. Grain boundary alpha hardness does not appear to be affected by matrix hardness at thicknesses of 15.8μ or greater.

The age hardening behavior of alloy #2 is being investigated by electron microscopy and hardness measurements. A technique has been developed to evaluate systematically the complex diffraction patterns characteristic of the $\alpha+\alpha'+\beta$ structures remaining after heat treatment. Observations have been made on the structure and morphology of the martensite in the as-quenched and 5 minute aged specimens. An alternate mechanism for void nucleation and growth is presented.

DD FORM 1 NOV 65 1473 (PAGE 1)

S/N 0101-807-6801

I-A

UNCLASSIFIED

Security Classification

UNCLASSIFIED

Security Classification

14 KEY WORDS	LINK A		LINK B		LINK C	
	ROLE	WT	ROLE	WT	ROLE	WT
Titanium Alloys High Strength Titanium Alloys						

DD FORM 1 NOV 68 1473 (BACK)

(PAGE)

UNCLASSIFIED

Security Classification

STRENGTHENING MECHANISM OF HIGH STRENGTH TITANIUM ALLOYS

H. Margolin
M. A. Greenfield
E. Levine
I. Greenhut
H. Park

Contract No. F33615-71-C-1301

I-C

FOREWORD

This report was prepared by New York University, Engineering Research Division under USAF Contract No. F33615-71-C-1301. This contract was initiated under Project No. 7351, "Metallic Materials", Task No. 735105 "High Strength Metallic Materials". The work was administered under the Metals and Ceramics Division, Air Force Materials Laboratory, Paul L. Hendricks (AFML/LLP), project engineer.

This report covers work conducted from December 1970 through December 1971.

The authors express their appreciation to Mr. I. Perlmutter, Dr. C. Pierce and Mr. P. Hendricks for their continuing interest and encouragement. The authors are indebted to Dr. T. Rosald for carrying out the fracture toughness tests and providing necessary auxiliary information. They also thank Mr. T. Cooper and Mr. V. DePierre for their assistance in the materials processing.

This technical report has been reviewed and is approved.

I. PERLMUTTER
Chief, Metals Branch
Metals and Ceramics Division
Air Force Materials Laboratory

Table of Contents

List of Tables

List of Illustrations

List of Illustrations (Continued)

I. Introduction

A. Status at the end of the Previous Contract

During the past year under USAF Contract No. F33615-70-C-1297 the study of factors affecting fracture toughness, void formation and growth, the ductility in an α-β titanium alloy, Ti-5.25Al-5.5V-0.9Fe-0.5Cu had been continued.

The results[1] may be summarized as follows:

1. Void Formation and Growth

a. Fracture of the equiaxed (E) and Widmanstätten plus grain boundary alpha (W+G.B.) morphologies does not occur by void coalescence but by unstable intergranular crack propagation.

b. The following equation relating fracture stress in both morphologies to longest crack at fracture was derived

$$\sigma_{f\,corr}^{E,\,W+G.B.} = 160.5 + 26.0\,L^{-1/2} \qquad [1]$$

where $\sigma_{f\,corr}^{E,\,W+G.B.}$ = fracture stress corrected for necking for both E and W+G.B. structures in Ksi

L = crack length at fracture in mm.

c. The following equations relating growth rate of the longest void to microstructural parameters were derived

$$G_L^E \text{ (mm/unit strain)} = .020 + (76\text{-}6.3D^{-1/2})(\lambda^{3/2} - 2.4\times10^{-4})$$

$$\text{for } \lambda^{3/2} \geq 2.4\times10^{-4},\ \text{mm}^{3/2} \qquad [2]$$

where G_L^E is the growth rate of the longest crack in an E morphology

D is the beta matrix grain diameter in mm

λ is the mean free path between alpha particles in mm

$$G_L^{W+G.B.} \text{ (mm/unit strain)} = D^{3/2} (8500\, \ell - 18.2)$$

$$\text{for } .0026 \leq \ell \leq .0055, \text{ mm} \qquad [3]$$

where $G_L^{W+G.B.}$ is the growth rate of the longest crack in a W+G.B. alpha morphology.

ℓ is the mean grain boundary alpha traverse thickness.

d. A mechanism for void growth at grain boundary alpha-beta matrix interface was proposed in which slip in both alpha and beta was required. It was proposed that an anisotropy of void growth took place. Void growth was proposed to take place more rapidly at that end of the void where $(0001)_\alpha - \{110\}_\beta$ slip could promote void growth and more slowly where this slip would not assist void growth.

e. Plastic strain of a tensile specimen was found to terminate when a void, growing stably, was converted to an unstable crack. Instability occurred when the growing crack reached a critical size as defined by the equation given in item 2 below. Instability occurred at a lower strain the more rapid was the void growth rate.

2. Fracture Toughness

a. Fracture toughness equations relating K_Q values to microstructures, based on limited data, have been confirmed and are given in the following:

$$K_Q^E \text{ (Ksi}\sqrt{\text{in}}) = 43(\text{Ksi}\sqrt{\text{in}}) + \frac{0.4 \text{ (Ksi}\sqrt{\text{in. mm}})}{D \text{ (mm)}} \qquad [4]$$

where K_Q^E is the fracture toughness of equiaxed alpha structures

D is the beta matrix grain size.

$$\Delta K_Q \text{ (Ksi}\sqrt{\text{in}}) = 10.5 \left(\frac{\text{Ksi}\sqrt{\text{in}}}{\text{microns}}\right) [\ell(\text{microns}) - 2.6 \text{ (microns)}]$$

$$\text{for } 2.6 \leq \ell \leq 5.5 \text{ microns} \qquad [5]$$

where $\Delta K_Q = K_Q^{W+G.B.}(d) - K_Q^{E}(D)$;

$K_Q^{W+G.B.}(d)$ is the fracture toughness of a W+G.B. structure at a given beta matrix grain size and

$K_Q^{E}(D)$ is the fracture toughness of an equiaxed alpha structure at the same beta matrix grain size.

b. Data has been obtained for K_Q at constant alpha morphology but higher "beta matrix" yield strengths.

3. Predictions

If a solution and aging treatment is carried out to fix the yield strength at 165,000 psi, it is possible from an examination of microstructure to predict

a. fracture stress

b. strain at fracture

c. critical crack length at fracture

d. void growth rate to critical crack size

e. fracture toughness.

B. Present Program

The present program has several objectives:

1. Work will continue to develop a microstructure with the highest obtainable fracture toughness to 165 Ksi.

2. Development of a high yield-high fracture toughness processing procedure for alloy #2 for yield strengths above 165,000 psi. As part of this work, thermo-

mechanical processing is to be attempted.

3. Study the relationship between microstructure and fracture toughness in an alloy which can develop strengths higher than alloy #2. The alloy to be used is Ti-6Al-6V-2Sn-1Cu-1Fe-3Zr.

4. Investigate in alloy #2, Ti-5.25Al-5.5V-0.9Fe-0.5Cu, the relationship between the aged beta matrix behavior and fracture toughness with the aid of electron microscopy.

5. Work to confirm previously derived void growth rate equations for W+G.B. structures by interrupted tensile tests.

II. Experimental Program

A. Alloy Preparation

Two 12 pound ingots of Ti-5.25Al-5.5V-0.9Fe-0.5Cu were prepared by double arc-melting in vacuum. The first melt was made by joining a total of thirty 200 gram compacts, each containing the desired alloy content. The compacts, 1-1/2 inch in diameter were joined into three electrodes of approximately 25 inches in length. These compacts were consumably melted in a vacuum of 1 μ to produce ingots 2-5/16" in diameter; three of these ingots were joined and consumably melted to form the final ingot of 3-3/4" diameter.

B. Processing

1. Bar M was forged from 3-1/4" diameter to 2-1/4" diameter at 1750°F, from 2-1/4" diameter to 1-3/8" diameter at 1600°F, then swaged from 1-3/8" diameter to .718"diameter at 1400°F. It was then heat treated at 1150°F-1hr. and swaged at 1150°F. Five sections were given a 35% RA and one section a 22% RA.

2. Bar L was forged from 3-1/4" diameter to 1-3/8" diameter at 1600°F and then swaged from 1-3/8" diameter to .609" diameter at 1400°F. All swaging was carried out at Wright-Patterson Air Force Base.

3. Hardness specimens were taken from bars of alloy #2, heat treated and swaged to a diameter of .455" in an earlier investigation. For microhardness measurements specimens were taken from Bar M.

C. Heat Treatment

1. All specimens were rough machined prior to heat treatment. Heat treatments were carried out in a vacuum furnace at a pressure of one micron or less. Although the heat treatments for each series were varied to form different morphologies, the last solution treatment in each case was one of 1625°F-W.Q. This was followed by an 1150°F-1hr. A.C. age. The temperature was controlled to ±10°F. At the end of a solution treatment the furnace was flooded with argon, the specimens removed and water quenched. The specimens were air cooled following aging.

2. Hardness specimens were cut to 3/8" lengths and heat treated for 3 hours at 1625°F prior to aging treatments at 950, 1000, 1150 and 1250°F.

3. For the microhardness tests W+G.B. alpha structure specimens after heating into the beta field at 1725°F for 30 min. were water quenched then reheated to 1625°F for times from 1-13 days to establish the desired grain boundary alpha thickness and again water quenched. These specimens were then aged at 915, 1150 or 1250°F to obtain desired matrix hardnesses.

Equiaxed alpha structures were obtained by heating as-swaged bars at 1625°F for times from 20 hrs to 10 days followed by water quenching. Equiaxed alpha specimens were aged only at 1150°F.

D. Machining and Testing

1. Following heat treatment, tensile specimens were finish machined to standard ASTM .250" dia. 1" gauge length. These were tested on a Tinius Olsen hydraulic unit with a microformer extensometer and strain rate pacer. The strain rate employed was in the range .003-.005 in/in/min.

2. Fracture toughness specimens - Three point bend tests were used on fatigue cracked charpy blanks to determine K_Q values. According to ASTM testing recommendations, a minimum specimen dimension of 2.5 $\left(\frac{K_{IC}}{\sigma_{y.s.}}\right)^2$ would require for the highest fracture toughness values encountered in earlier work, a minimum specimen size below the crack of 0.55". For the largest values of fracture toughness in the present work the dimension is .194". The depth below the fatigue crack in specimens tested was 0.26".

3. Hardness specimens were ground on a water cooled rotary grinding wheel then polished on emery paper to 400 grit.

4. Microhardness specimens were ground to remove about 0.5 mm. Specimens were ground to 600 grit and ther were electropolished and etched prior to indentation.

E. Metallographic Examinations

1. Electron microscope foils were prepared by cutting sections off a hardness specimen, pre-grinding on a rotary grinder, polishing down to 400 grit paper. then thinning to the final foil size using a potentiostatic electro-polishing setup at -30 to -40°C.

Foils of the as-quenched and 5 min at 1150°F hardness specimens

were examined and subsequent electron micrographs and diffraction patterns were taken at a magnification of approximately 40,000X.

2. All specimens for optical microscope examination were prepared by grinding and polishing down to 400 grit paper followed by electropolishing and etching.

F. Measurements

1. All measurements of microstructural constituents were made using the Hurlbut counter.

2. Vickers hardness measurements were made using a Zwick hardness tester with a 10Kg load. Three hardness indentations were made per specimen. The rate of descent of the indenter was kept constant for all tests. Each datum point represents the average of these three indentations.

3. A Bergsman hardness tester with a 5 gram load was used to determine microhardness. A load of 5 gr. permitted hardness measurements to be made for G.B. and E alpha traverse thicknesses as small as 5 μ. The rate of approach of the specimens to the indenter was kept constant by using a motor to control the rate of descent of the stage. The duration of application of the load was maintained constant at 15 seconds. From 20 to 55 indentations were made to determine the hardness of a given constituent, alpha or aged beta. In this case, alpha particles were picked at random.

In the course of the experimental work it was decided to measure the hardness of grain boundary alpha of a series of constant thicknesses, designated random section thickness. From 5 to 21 indentations were used to determine hardness for a given thickness.

4. Diffraction patterns were analyzed for d-spacing and zone-axis identifications as follows:

a) All diffraction patterns were taken at a standard magnification over which the electron microscopy camera constant had been calibrated. The camera constant was found to be 25.2 mm-Å. The value of R, the distance on a photographic plate from the transmitted beam to a diffraction spot, in the expression $L\lambda = dR$ was then measured directly from the diffraction patterns, where $L\lambda \equiv$ camera constant, L being the plate to specimen distance and λ the wavelength of the electron beam. R was measured to the nearest tenth of a mm using a finely calibrated ruler and in some cases a calibrated magnifying eye piece.

b) Lattice spacing could only be approximated due to instability in the microscope which leads to minor variation in the camera constant. These also could not be directly compared to the calculated d-spacings since the lattice parameters of all the phases present could only be approximated in the absence of x-ray diffraction data. The following method was devised to confirm the postulated zone axis and associated d-spacings. The Burgers relationship

$$(0001)_\alpha \parallel \{110\}_\beta$$

$$\langle 11\bar{2}0\rangle_\alpha \parallel \langle 111\rangle_\beta$$

is assumed to be valid. On this basis, transparent stereographic projections were constructed. 111 and 110 projections were constructed as well as a standard 0001 projection. By superimposing these projections in such a way as

to satisfy the Burger's relationship one may predict, 1) all the possible zone axes which will contain strong reflections from more than one phase; 2) the symmetry of each of these axes; and 3) their relative position with respect to one another. Thus from a single diffraction pattern, one can postulate the origin of the reflections and then confirm it by tilting to the other axis predicted by the projection. After identifying the origin of the reflections in the diffraction patterns, dark field electron micrographs were then used to examine the structure and morphology of the as-quenched martensite.

III. Results and Discussion

A. Fracture Toughness at Increased Yield Stresses

1. Effect of Heat Treatment

Specimens of alloy #2 were heat treated at 1625°F and aged 1hr at 915°F to raise the yield stress. The results are shown in Table I which includes data reported during the 1971 Annual Report[3]. Yield strengths of 194-196 Ksi were obtained for E alpha structures and yield strengths of 181-187 Ksi were obtained for the W+G.B. structures.

From the microstructural parameters the fracture toughness could be calculated for a yield strength of 165 Ksi from equations [4] and [5]. The results are shown in Fig. 1, a plot of fracture toughness vs yield strength. With the exception of specimen F-17, the slope of the decrease in fracture toughness, as yield strength is raised above 165 Ksi, is essentially the same for both the E and W+G.B. morphologies. Since fracture toughness consists of a grain boundary contribution in E alpha and a grain boundary plus a grain boundary alpha thickness increment in the W+G.B. alpha structure this implies

that the matrix behavior may be controlling both types of contributions to fracture toughness.

As will be shown later[4] the hardness of alpha depends on the hardness of the beta matrix. The harder is the beta matrix the harder is the alpha for the same alpha morphology and size of alpha particle. Thus when the matrix is strengthened the grain boundary alpha is strengthened. This is in agreement with the information provided by fracture toughness data. However, no direct comment can be made on how ΔK_Q will vary with grain boundary alpha thickness at higher strength levels.

Fig. 2 shows a plot of fracture toughness versus S_v (=2/D), grain boundary area per unit volume, for the 195 Ksi yield strength equiaxed alpha structure. Also shown is the K_Q-S_v line for the 165 Ksi yield strength. If the point for F-17 is not considered, the slope of the 195 Ksi yield K_Q-S_v straight line is almost the same as that of the 165 Ksi yield strength material. When the grain size effect is zero, the difference in fracture toughness between the two curves is 41 Ksi/in. This difference becomes slightly larger as grain size decreases because of the steeper slope of the 165 Ksi K_Q-S_v line.

It is possible to make a rough check of the contribution of grain boundary alpha to the fracture toughness at a yield strength of 185 Ksi. If the reduction in fracture toughness, as yield strength is increased, is considered to be linear, then the fracture toughness at zero contribution from grain size would be 15 Ksi/in at 185 Ksi yield stress. A dashed line has been drawn in Fig. 2 with the same slope as the 165 Ksi K_Q-S_v line for the 185 Ksi yield. This represents the grain boundary contribution to fracture toughness. This

line can be used to calculate the K_Q^E data that corresponds to the $K_Q^{W+G.B.}$ data of Table I. For example, the grain size of sample F-21, Table I, is 138 microns. The corresponding 2/D value is 14.5 mm^{-1}. From Fig. 2, the corresponding K_Q^E value is 16.2 as listed in Table II and the difference between this value and $K_Q^{W+G.B.}$ is listed as ΔK_Q. A plot of ΔK_Q of Table II vs ℓ is shown as a full line in Fig. 3. Also shown in Fig. 3, as the dashed line, is the ΔK_Q vs ℓ curve for the 165 Ksi yield.

Two observations can be made from Fig. 3. The plateau, where the increment to fracture toughness provided by the grain boundary alpha remains constant, is essentially the same as that of the 165 Ksi yield case. The ΔK_Q plateau value for the 165 Ksi yield is 26.8 Ksi/in compared to 24 Ksi/in in the present case. However, the grain boundary alpha contribution does not go to zero at a grain boundary alpha thickness of 2.6 microns, as in the 165 Ksi yield case. Rather, it goes to zero at some lower value, undefined because of the limited data available at this writing. Thus at yield strengths above 165 Ksi it appears that grain boundary alpha can continue to make a contribution below a thickness of 2.6 microns.

At this point it is desirable to depart momentarily from the discussion on fracture toughness to develop some ideas on void growth in alpha. This information will be used in a discussion of the role of grain boundary alpha on fracture toughness.

It has been frequently observed that void growth extends only partially into equiaxed alpha before stopping. This can be seen in Fig. 9 of[1] and Fig. 4 of[3]. When there is no void at the α-β interface and the equiaxed particle is

sufficiently small (10 μ or less, according to the hardness data to be presented), it is essentially fully constrained. Its flow strength is raised to the flow strength of the beta matrix. When a void forms, the flow strength in alpha at the alpha-void surface drops to the flow strength of unconstrained alpha. Away from the alpha particle-void interface the constraint effects increase and the flow strength of alpha increases until at some position in the particle it is fully constrained again.

As the void grows larger, the region of alpha over which the stress drops to the unconstrained alpha flow strength also enlarges. A point is reached where the stress in the alpha particle, near the interface opposite the void, does not return to the stress required for flow to take place in the constrained, higher strength area. Because flow cannot take place, the void stops growing.

A similar effect occurs when a crack meets a grain boundary alpha particle, as in Fig. 4a, i.e., the flow strength of the alpha adjacent to the crack tip decreases. Flow takes place more readily where the constraint effects have been removed, hence the crack turns to follow the alpha-beta interface. Flow at the crack tip removes material at the interface as shown in Fig. 5 which is Fig. 15 of [3]. The crack will not move completely into the alpha because slip will become more difficult as the opposing alpha-aged beta interface is approached. Therefore, the crack will ramain at the alpha-aged beta interface as has been shown[4].

The hardness data to be presented suggest that grain boundary alpha is fully constrained to the strength of beta at a thickness of 5.5 μ. Yet in the region of 2.6 - 5.6 μ thickness grain boundary alpha continues to provide a ΔK_Q

increment to fracture toughness. This contribution to fracture toughness must arise from regions A and B of Fig. 4b. Both of these regions must contribute to stress relief at the crack tip. The extent of this stress relief will depend on whether the dislocations moving in alpha from the vicinity of the crack tip can enforce slip in the aged beta.

Prior to reaching the grain boundary alpha particle, the strain field of the crack tip has caused hardening of both the alpha and aged beta matrix. For flow to take place in the matrix adjacent to the interface, the pile-up stress at the alpha-aged beta interface must be sufficient to overcome this hardening. If the pile-up is just barely sufficient, local flow will take place in the aged beta. If the pile-up increases, then, although the stress may not increase, the extent of flow in the matrix will increase and stress relief of the crack tip will be more effective.

Returning to Fig. 3, the dashed curve referring to 165 Ksi yield could then be interpreted in the following way. Below a grain boundary alpha thickness of 5.5 μ the pile-up of dislocations is diminishing in size and the extent of flow in the beta is diminishing. At 2.6 microns the flow in the beta is so small as to make no contribution to the fracture toughness and the alpha, in terms of fracture toughness, behaves as if it were beta. On the other hand, when the thickness of grain boundary alpha is 5.5 μ or greater, the pile-up of dislocations is sufficient to cause more than just local slip in the matrix and slip can continue extensively away from the interface. Increasing the thickness beyond 5.5 μ does not increase the extent of matrix flow at the side opposite the crack tip and hence no increase in fracture toughness takes place.

Fig. 4b shows a region ahead of the crack where constraint effects are suggested as not being fully established. If this region does in fact exist, it is likely to play an important part in the stress relief, since this region would feel the constraint effects most strongly. Thus if the yield strength of the matrix increased above 165 Ksi for a given applied stress, producing plastic flow, the stress in this region would not decrease to the same extent as at 165 Ksi, because of the greater constraint of the harder matrix.

When the yield strength of alloy #2 is raised to 185 Ksi, the fracture toughness decreases, Fig. 1. This is manifested by a decrease in load required to fracture the specimen. This drop in load does not necessarily mean that the stress in alpha at the crack tip region B of Fig. 4b is also lower than that for the 165 Ksi material. This possibility arises because of the constraint effects discussed earlier.

If the stresses in alpha were higher, despite the lower load, then the thickness at which the pile-up stress in alpha could cause extensive flow in beta would decrease. This follows, since for a given number, n, of dislocations in a pile-up, the stress at the head of the pile-up is n times the effective shear stress. Thus a contribution of alpha to fracture toughness could be realized at smaller thicknesses. The plateau, along which further increase in thickness no longer produces an increase in fracture toughness, would extend to an alpha thickness below 5.5 μ. The shift of the 165 Ksi ΔK_Q curve (dashed line of Fig. 3) to the lower alpha thickness values of the 185 Ksi yield (full line of Fig. 3) is in agreement with this concept.

A word of caution must be given here. More data for the 185 Ksi yield

strength are needed before it can be considered that the relationship is fully established.

A further implication of this discussion is that the thickness of alpha at which a contribution can be made to fracture toughness not only depends on the yield strength of the matrix, but also the strain hardening in the vicinity of the interface. If the strain hardening rate is low then grain boundary alpha will be able to make a contribution at a smaller thickness. Thus the position of the curves of Fig. 3 will not only depend on yield strength but on strain hardening rate as well.

Widmanstätten alpha, when thick enough, should also provide an increment to fracture toughness. Gerberich[6] has shown a crack proceeding along a Widmanstätten aged beta interface in Ti-6Al-4V. The available evidence[4] indicates that the crack in a fracture toughness test propagated on the unoriented alpha side of grain boundary alpha.

The Widmanstätten alpha has, of course, no unoriented side. However, crack extension would be easier if the crack traveled along the path shown in Fig. 6b rather than in Fig. 6a.

If this were true, the crack in Fig. 6b would experience constraint effects quite similar to those for the grain boundary alpha case. Consequently one would expect that essentially the same thickness of Widmanstätten alpha would be required to produce the same fracture toughness increments as grain boundary alpha.

If the Widmanstätten alpha were appreciably thinner than the grain boundary alpha no crack propagation along Widmanstätten alpha would be found.

If the thicknesses were similar, the crack path would alternate between the two types of alpha.

It must be recognized that the preceding discussion of the increments to fracture toughness provided by grain boundary and Widmanstätten alpha have referred to aged beta matrices whose strengths are considerably greater than those of alpha when the latter is free of constraints. It is not yet known whether or not the increment is relatively independent of the characteristics of the matrix or how it will vary with either matrix properties or the intrinsic behavior of the alpha itself.

Because of the limited data and the necessity for making assumptions as to the position of the 185 Ksi K_Q-S_v line, the previous discussion must be considered tentative.

B. Fracture Toughness and Warm Working

An attempt has been made to determine the effect of warm working material which had previously been heat treated to produce 165 Ksi yield stress. As was pointed out in the experimental procedure section, the warm working was carried out at 1150°F. The results are presented in Table III.

Table III indicates that a reduction of 35% at 1150°F has had very little effect on the yield strength of alloy #2. This may be due to somewhat greater work being introduced into the outer portions of the bar which were removed during machining. However, it is also probable that some precipitation of alpha, which took place during swaging, effectively served to reduce the dislocation density and hence the strength of the bar, thus offsetting the cold working effects. Some evidence for alpha precipitation during warm working

is shown in Fig. 7. Here the equiaxed alpha has a mound-like appearance because of precipitation adjacent to the primary alpha.

During the examination of specimens of bar M it was found that a bi-modal grain size had been formed. This bi-modal grain size was found after heat treatment above the β-transus and is shown in Fig. 8, specimen MCV. It has also been found in Bar L. This problem has not previously been encountered.

The bi-modality was more evident at the center of the specimens than it was near the surface. This suggests that it developed as a result of the swaging process. Bars L and M were the only ones which were swaged so extensively, i.e. from 1-3/8" to either .713 or .609".

The grain size measurements reported in Table III are the average grain size. It is not known whether the bi-modality exists in the equiaxed specimens.

The microstructures of the grain boundary alpha morphology frequently show very little alpha. The grain or sub-boundaries are outlined by a precipitate type structure which probably formed as a result of working and heat treating at 1150°F. This structure is so uncharacteristic of structures previously encountered that no comment will be made regarding the fracture toughness.

Insofar as the equiaxed alpha structure is concerned, the fracture toughness is basically that of an extremely large grain size in which there is no contribution of grain boundaries. It is not possible to determine grain size in these specimens unambiguously because the process involves heating just

below the beta transus. Since these specimens have been worked, recrystallization may occur on heating to the required temperature.

It is possible, at this point, only to say that warm working at 1150°F is not a suitable process to raise the yield strength of this alloy.

C. Hardness of Alpha

1. General Observations

Prior to the work undertaken here no systematic investigation of the hardness of alpha in an alpha-beta alloy had been undertaken. Scratch tests had indicated that alpha was softer than beta[4]. Fracture toughness data[4] had suggested that grain boundary alpha was constrained to strengths above what would be expected if alpha were not imbedded in a harder matrix. Direct confirmation of the elevation of the flow strength of alpha by beta was obtained by a tensile test[4].

Because of the paucity of data and the need to understand the interaction between alpha and the aged beta matrix, hardness tests of alpha were undertaken. It was expected that the hardness of alpha would depend on the hardness of beta. Accordingly, microhardness measurements were recorded for the aged beta matrix as well. Results for grain boundary alpha structures are given in Figs. 9a, b, and for equiaxed alpha structures in Fig. 10. The same specimens as were used to determine as-quenched hardness were employed to obtain the effects of aging.

Fig. 9a indicates that the hardness of beta decreases with increasing alpha thickness for both the as-quenched and aged condition. There is no a priori reason to expect such behavior and the hardness of beta shown in Fig. 9b, par-

ticularly the as-quenched data shows no such behavior. Since the specimens of Fig. 9a were wrapped in titanium sheet prior to solution treatment, it is believed that retardation of quenching by the protective sheet gave rise to the fortuitous results.

Fig. 9a shows that the hardness of alpha decreases with increasing thickness and with decreasing beta hardness. It is to be expected that the decrease in beta hardness would assist any decline in alpha hardness due to increasing alpha thickness. It is of interest to note that the hardness of alpha where the specimen has been aged is raised to values above that of beta in the as-quenched state, compare curves B and C of Fig. 9a.

The as-quenched data of Fig. 9b, curves C, and D, show that the hardness of grain boundary alpha decreases with increasing thickness at constant matrix hardness. Some variation in the hardness of the aged beta can be seen, curve A. However, since this variation is smaller than that of curve A, Fig. 9a, the drop in hardness with increasing grain boundary alpha thickness, curve B, of Fig. 9b, is smaller than that of curve B, Fig. 9a.

Fig. 10 shows that the hardness of equiaxed alpha is raised when the hardness of the matrix is increased. However, the decrease in equiaxed alpha hardness with increasing size is much smaller than that of grain boundary alpha.

An attempt was made to determine the effect of both beta matrix hardness and alpha size on the variation of alpha hardness. The results are shown in Fig. 11 for grain boundary alpha and in Fig. 12 for equiaxed alpha. A wider range of aged beta matrix hardness was obtained for the grain boundary alpha structures by varying both aging temperature and time. The data for Fig. 12

was obtained from the natural variation which occurred in the aged beta matrix after aging at 1150°F.

The data of Fig. 11 fall in a band roughly 60 VHN wide, but again confirm that the hardness of alpha increases with increasing matrix hardness. Within the band the highest hardness appears to be associated with the smallest alpha thickness. Thus it would appear that the range of hardness obtained is related to the variation in alpha thickness as would be expected from Figs. 9a, b. In agreement with the data of Fig. 10 the data for equiaxed alpha, Fig. 12, if superimposed on the data of Fig. 11, would be found to lie in the vicinity of the upper portion of the band in Fig. 11.

Examination of the data suggests that,for a given matrix hardness, when grain boundary alpha is thicker than 5-7 microns,it tends to be softer than that of equiaxed alpha of the same thickness or diameter.

Although the data of Fig. 11 appear to fall within a band which had uniform width, intuitively it did not seem reasonable that the variation in hardness of beta should produce essentially a constant range in the hardness of alpha.

2. Hardness of Grain Boundary Alpha at Constant Matrix Hardness

If there is a variation in grain boundary alpha thickness for a given traverse thickness, the actual average hardness obtained depends on the thickness of the alpha selected for hardness indentation as indicated earlier. Let us consider the geometrical effects which are involved. Let us assume that the grains are spherical and that,when alpha precipitates around the grain boundary,it forms a spherical shell of constant thickness as shown in Fig. 13.

The thickness of alpha, as it would appear on the plane of polish, would depend on the position of the intersecting plane with the grain.

The smallest alpha thickness would be found when the plane of polish intersected the grain along a diameter, intersection AB, Fig. 13. The largest alpha thickness would occur when the plane of polish passed through the tangent point indicated by, intersection EF, Fig. 13. Since the hardness indenter would penetrate the alpha in a direction perpendicular to the plane of polish the thickness of alpha below an indenter would be greatest along AB and least along EF.

If the hardness of the aged beta matrix is greater than the alpha, free of constraints, and if the thickness of alpha varied only because of the position of the sectioning plane, then as alpha thickness on the plane of polish increased the hardness of alpha would increase because the influence of beta would be felt most in the alpha which appeared thickest. The variation in hardness of alpha would increase with apparent alpha thickness as shown in Fig. 14. As will be shown, the hardness of alpha actually follows the dashed line. This behavior then indicates that the change in hardness with alpha thickness is not due to support by the beta lying below the indented alpha.

It is of interest at this point to determine what the thickness of alpha on the plane of polish represents. If a line is passed randomly through a sphere, it can be shown that the average length of this chord is ch, Fig. 13, where

$$ch = 4/3\ r,$$

r being the radius of the sphere.

The plane of polish can be considered as a random plane passing

through the grains. Thus on the average, the plane of polish can be considered to pass through the grains along the position cd. When considering the thickness of alpha on the plane of polish the thickness cd is the minimum thickness in the plane of polish or the "random section thickness". An average alpha thickness so measured represents the average of different alpha thicknesses intersected at different positions.

Fig. 15 is a plot of VHN of alpha at various constant matrix hardness values and constant average alpha thickness of 8.5 μ corresponding to cd of Fig. 13. The various alpha thicknesses shown in Fig. 15 were found in the spread of alpha thicknesses resulting in the 8.5 μ average thickness. Six matrix hardnesses were used. The data indicate that as the alpha thickness decreases the hardness increases. From the previous discussion, this behavior is due to constraint effects of the beta matrix imposed along the sides of the grain boundary alpha.

It can be seen that five of the six hardness-thickness lines intersect at a common thickness of 15.8 μ. Initially this would appear to be the grain boundary alpha thickness at which the hardness of the matrix has no further influence. This is immediately ruled out on two counts. Fig. 10 shows that at an equiaxed alpha traverse diameter of 20 μ (which if converted to actual diameter according to the discussion pertaining to Fig. 13 would make the equiaxed alpha particle still larger than 15.8 μ), the hardness of alpha varies considerably with matrix hardness. The second count is the behavior of the 267 VHN matrix data, which show Vickers hardness values below 224 which corresponds to the 15.8 μvalue.

The common intersection would rather suggest that at a thickness of 15.8 microns the pile-up stress at the oriented side of the grain boundary alpha is sufficiently large as to be able to overcome the resistance offered by the hardness of beta in the range of matrix hardnesses encountered. In this connection it is of interest to note that if the size of the impression is calculated from the VHN of 224 at 15.8 μ thickness, the distance of the impression from the alpha-aged beta interface falls in the range of 4.7 to 5.6 μ, see Fig. 16.

The distance corresponds to the thickness of alpha at which the constraints of the matrix are postulated to be overcome at 165 Ksi yield. However, since the indentation becomes smaller in size below the surface of observation, the sizes of Fig. 16 represent the minimum distance of the impression from the interface, but the distances at which maximum stress would be applied at the interfaces.

It is of interest to consider the data of the GB - 3 series which shows hardness values below 224 VHN of 15.8 μ grain boundary alpha. This is taken to mean that when the beta is sufficiently soft other factors than matrix constraint may influence alpha hardness. Such a factor may well be the orientation of alpha with respect to the surface.

Finally it is of interest to consider the thickness at which the hardness of alpha becomes equal to the hardness of the matrix. This can be determined in two ways: 1) by drawing a horizontal line corresponding to the matrix hardness for a given series and determining the alpha thickness from the intersection with the hardness-thickness curve and taking the average of the intersec-

tion, or 2) by first plotting a series of curves of VHN α vs VHN β at constant alpha thickness, Fig. 17; next determining the slope of these curves and plotting the slope vs alpha thickness, Fig. 18; the thickness at which the slope is unity, is taken to be the thickness at which grain boundary alpha always has the same hardness as beta.

The average of the intersections of Fig. 15 is 4.6 μ, the range being 3.4 to 6.2 μ, and the thickness at which the hardness of alpha is always the same as beta from Fig. 18 is 4.8 μ. The size of the impressions as a function of matrix hardness is as follows:

Aged Beta Matrix VHN	Diagonal of Impression, μ	Length of Side of Impression, μ
521	4.2	2.82
442	4.56	3.23
352	5.11	3.62
340	5.21	3.69
311	5.46	3.87

The diagonal length is approximately equal to or greater than the alpha thickness for VHN of 442 or less. At a VHN of 521 the diagonal is not much smaller than the alpha thickness. Thus it can be said that the hardness of alpha becomes equal to that of the aged beta matrix when the diagonal of the impression is approximately the same width as the random section thickness. This in turn indicates that the hardness impression cannot distinguish the difference between alpha and the matrix and thus that the alpha is fully constrained at 4.8 μ.

D. Age Hardening Behavior

A study of the age hardening behavior of alloy #2 for a 1625°F solution treatment and an 1150°F age is being carried out to ascertain the relationship

between fracture toughness and matrix behavior.

1. Hardness Curves

Fig. 19 shows the age hardening behavior of alloy #2 after aging at 950, 1000, 1150 and 1250°F for equiaxed alpha structures. It is interesting to note that maximum hardness is reached after aging two minutes at 950, 1000 and 1200°F. This suggests the possibility that this maximum is reached during heating to the aging temperature. A preliminary electron microscope examination of the as-quenched microstructure is presented in the following.

E. Electron Microscopy Study of Age Hardening Mechanism

1. Evaluation of Diffraction Patterns

The complexity of the microstructure made it impossible to find any one region from which a clearly defined cross grating pattern could be obtained for indexing purposes. The technique of overlaid transparent stereographic projections was therefore developed to aid in indexing these complex diffraction patterns. In the absence of precise values for the lattice parameters and the difficulty in finding a single complete cross grating pattern within a specific martensite platelet, the only way to make definite identification of a given pattern is to show that all proposed or tentatively labelled reflections are consistent with one another, provided that the Burger's orientation relationship is obeyed.

Fig. 20 shows such a pattern where the overlapping α' zone axes have been identified and labelled A, B, D. The common β zone axis is of the [311] type. Zone axis C is higher order and, because the only low order reflection (110) is superimposed on the α'' (0002) reflection it is not separable from alpha. Fig. 21 shows an overlaid transparent stereographic projection

with the zone axes A, B, C and D indicated. The overlay satisfies the Burger's relationship. This technique also allows one to tilt away from an orientation already identified, for the purpose of separating out reflections. With this technique, different regions may be delineated in dark field images and identification of patterns composed of only one β reflection and one α' reflection is aided.

2. Characterization of Overall Microstructure

Figs. 22 and 23 show a typical area of the as-quenched foil. It consists of beta grains with a large percentage of martensite and equiaxed alpha particles enclosing grains of beta with a grain diameter approximately equal to the mean free path between alpha particles. Diffraction pattern analysis showed that a Burger's relationship existed between several equiaxed alpha particles and the beta grain. One example of this is shown by the circled region of Fig. 22a and the corresponding diffraction pattern, Fig. 22b. Frequently, the equiaxed alpha particles were connected by an alpha bridge, as shown in Fig. 24, which is an enlargement of the lower portion of Fig. 23.

3. Nature of Martensite

All martensites observed to date could be indexed as the usual α hexagonal variety, although frequent observations of split reflections in the as-quenched foil suggest that more than one c/a ratio is present. The several different morphologies of martensite all were observed to obey the Burger's relationship.

Fig. 25 is a typical bright field micrograph of a region within a β grain. It is characterized by a high residual dislocation density in both the

retained β and the martensite plates, although the latter are difficult to discern in bright field. Selected dark field micrographs on β and α′ reflections permits one to delineate the characteristics of the as-quenched structure. Thus the α′ in Fig. 26 may be seen to be of the lightning bolt variety at A. Larger martensite plates with a length equal to the grain diameter can be seen in Fig. 26 at B.

Fig. 27 is a dark field micrograph taken on a 112 β reflection. The regions of retained β are light and stand out clearly relative to the dark background. From the micrograph one can see that the retained β occupies approximately 10-20% by volume. The martensite plates which occupy the remainder of the region are, in general, quite small. Plates of two types could be observed. Those indicated by arrows in Fig. 27a have a thickness of 4000 Å and a length of approximately 1 μ. The second type, longer plates, not clearly visible in Fig. 27a are shown in Fig. 27b which is a dark field micrograph taken on an α′ reflection. The regions entrapped within the plates are martensite of a different orientation. Area D in Fig. 27a shows that what appears to be a large internally twinned plate is really parallel plates with small regions of entrapped β between them.Often small regions around the large equiaxed particles are devoid of α′ plates and consist of solely β as can be seen by examining region D in Fig. 27a.

F. Void Nucleation Mechanism

A mechanism involving a pile-up of dislocation in alpha to form an elastic crack which later is converted into a plastic crack was proposed earlier[1]. This is initially attractive and would fit the data. However, it suffers from the problem that only two to four dislocations would appear in the pile-up because

of the limitations of the beta yield strength and that this pile-up could easily be dispersed by cross slip.

An alternate mechanism is one in which compatibility requirements at the α-β interface break down permitting void nucleation to occur. Maintaining compatibility would be difficult if slip in alpha could occur extensively on a single system. Evidence for extensive slip on a single system in grain boundary alpha, even after the ultimate tensile strength has been reached, has already been published, see Fig. 11 of [4]. Similar observations have been made for both equiaxed and Widmanstätten alpha. As strain hardening occurs in the beta, the ability to accommodate this extensive planar slip on a single system would diminish. Observations of extensive planar slip in aluminum alloyed titanium have been reported in the literature[5].

References

1. M. A. Greenfield and H. Margolin: "Strengthening Mechanism of High Strength Titanium Alloys". Technical Report AFML-TR-70-43, Air Force Materials Laboratory, Wright-Patterson Air Force Base, Ohio, April 1970.

2. Fracture Toughness Testing and Its Applications, p. 133, American Society for Testing and Materials, Philadelphia, Pa., 1965.

3. M. A. Greenfield and H. Margolin: "Strengthening Mechanism of High Strength Titanium Alloys". Technical Report AFML-TR-71-48, Air Force Materials Laboratory, Wright-Patterson Air Force Base, Ohio, March 1971.

4. M. A. Greenfield and H. Margolin: "The Interrelationship of Fracture Toughness and Microstructure in a Ti-5.25Al-5.5V-0.9Fe-0.5Cu Alloy". Metallurgical Transactions 1971, 2, p. 841.

5. M. J. Blackburn and J. C. Williams: "Strength, Deformation Modes and Fracture in Titanium-Aluminum Alloys". Trans. ASM 1969, 62, p. 398.

6. W. W. Gerberich: "Some Observations on Crack Extension in Two Phase Materials", Trans. TMS-AIME, 1967, V. 239, p. 753

Table I

Fracture Toughness and Microstructure at Increased Yield Strengths

Equiaxed Alpha

Specimen Number	Pct. Primary Alpha	D Microns	d Microns	λ Microns	$\sigma_{0.2}$ Ksi	K_Q Ksi√in	Calculated K_Q at 165 Ksi Yield Strength Level * Ksi√in
F17	20.7	94	2.4	9.2	196	- 30.2	47.2
F16	23.2	85	2.6	8.6	165	- 46.2	47.7
F28	28.6	20	2.1	5.3	196	- 21.0	60.0
F26	26.4	24	2.3	6.4	196	- 15.5	63.0
I13	44.0	14	3.8	4.8	194	- 26.2	71.6

Widmanstätten plus Grain Boundary Alpha

Specimen Number	Pct. Primary Alpha	D Microns	ℓ Microns	$\sigma_{0.2}$ Ksi	K_Q Ksi√in	Calculated K_Q at 165 Ksi Yield Strength Level * Ksi√in
F21	30.2	138	2.2	181	- 26.7	45.9
F27	29.4	126	2.5	185	- 27.0	46.1
I7	28.1	113	6.4	187	- 37.9	77.0
I9	33.0	143	4.6	184	- 40.2	66.8

* Calculated from Equations [4] and [5]

Table II

ΔK_Q vs ℓ at Increased Yield Strength, 185 Ksi

Specimen Number	ℓ	$K_Q^{W+G.B.}$	Corresponding K_Q^E	ΔK_Q
F21	2.2	26.7	16.2	11.5
F27	2.5	27.0	16.5	11.5
I7	6.4	37.9	16.7	23.2
I9	4.6	40.2	16.0	24.0

Table III

Microstructural and Mechanical Properties for 1150°F Warm Worked Alloy #2

Specimen Number	K_Q Ksi/in	$\sigma_{0.2}$ Ksi	$\sigma_{f\,corr}$ Ksi	%R.A.	%Elong.	Ultimate Strength Ksi	D_β μ	ℓ μ	Heat Treatment
MBA	37.1	175	204	15.5	7.0	183			1725°F - 20m - W.Q. 1625°F - 4h - W.Q. 1150°F - 1h - A.C. 35%RA @ 1150°F
MBB	38.6	167	253	41.5	11.8	175	104	5.99	1725°F - 10m - W.Q. 1625°F - 16h - W.Q. 1150°F - 1h - A.C. 35%RA @ 1150°F
MCA	44.7	169	250	37.2	13.8	177	90	3.93	1725°F - 10m - W.Q. 1625°F - 4h - W.Q. 1150°F - 1h - A.C. 35%RA @ 1150°F
MCB	45.9	167	246	42.7	11.8	175	52.5	5.20	1725°F - 10m - W.Q. 1625°F - 16h - W.Q. 1150°F - 1h - A.C. 35%RA @ 1150°F
MDA-1	41.4	167	288	54.3	17.0	176			1625°F - 4h - W.Q. 1150°F - 1h - A.C. 35%RA @ 1150°F
MDA-2		166	208	19.8	9.0	175			1625°F - 4h - W.Q. 1150°F - 1h - A.C. 35%RA @ 1150°F
MDB	43.1	158	205	21.8	9.0	170			1625°F - 16h - W.Q. 1150°F - 1h - A.C. 22%RA @ 1150°F

D_β = Beta matrix grain size

ℓ = Grain boundary α thickness

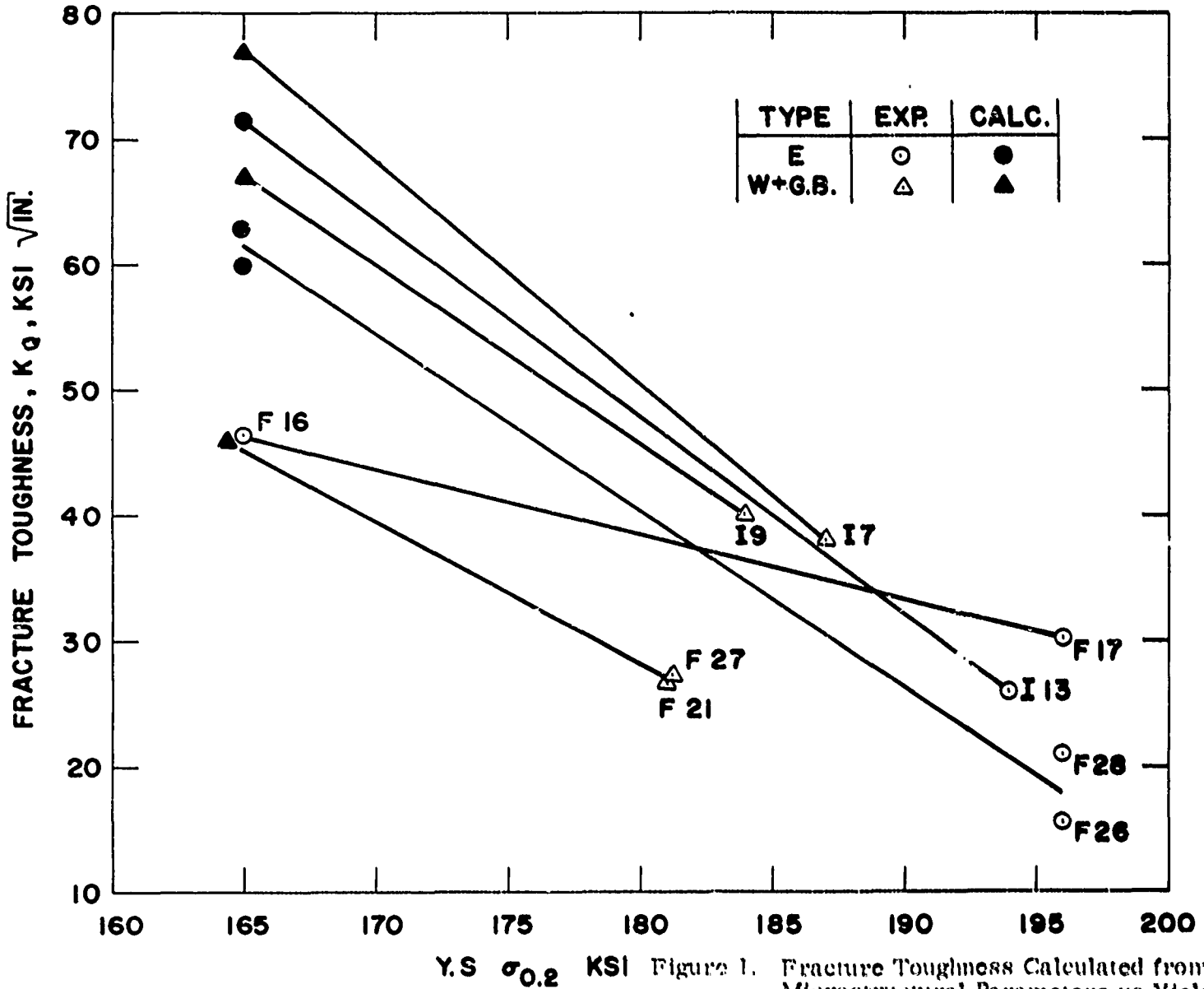

Figure 1. Fracture Toughness Calculated from Microstructural Parameters vs Yield Strength.

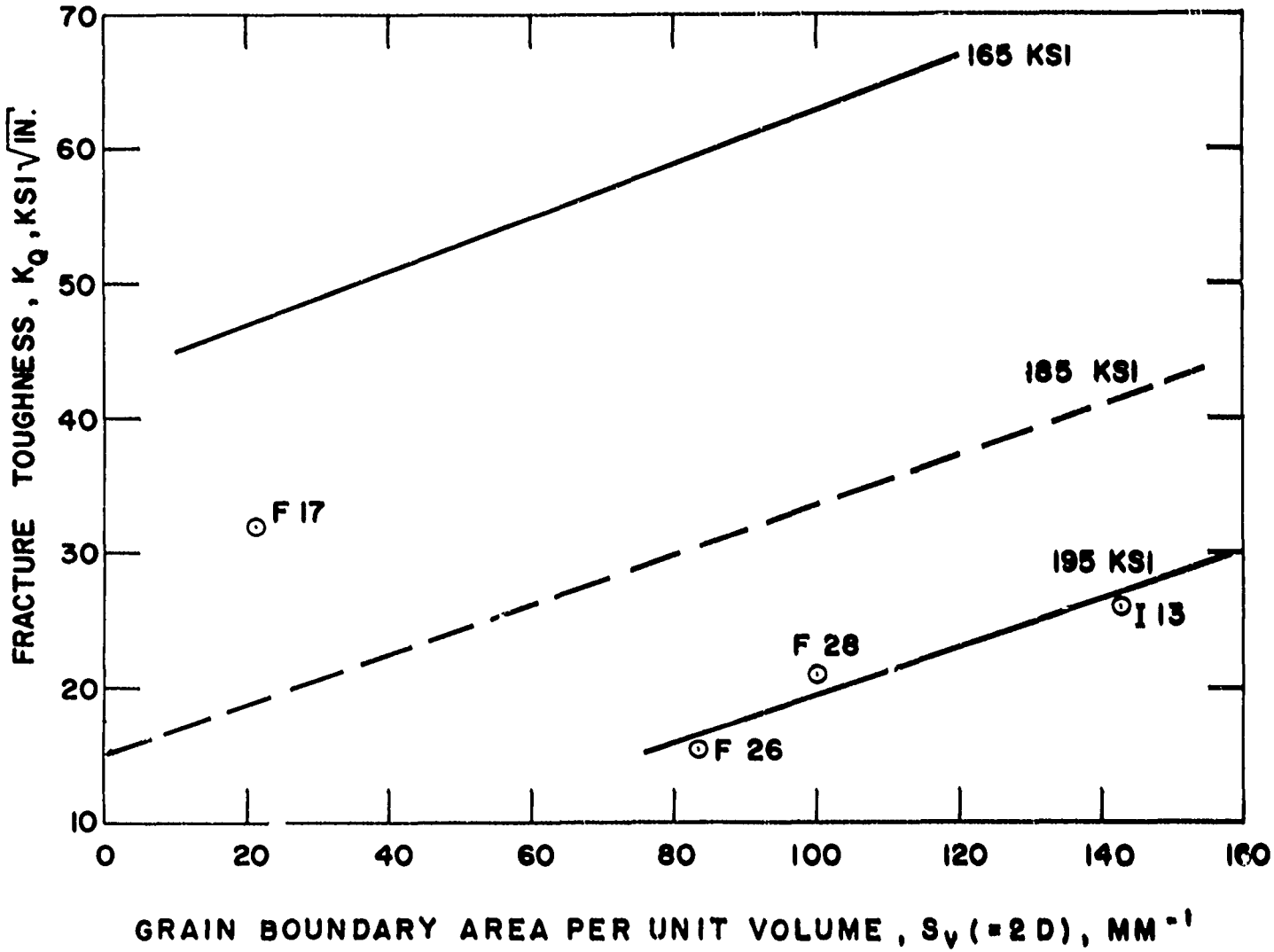

Figure 2. Fracture Toughness vs Grain Boundary Area Per Unit Volume.

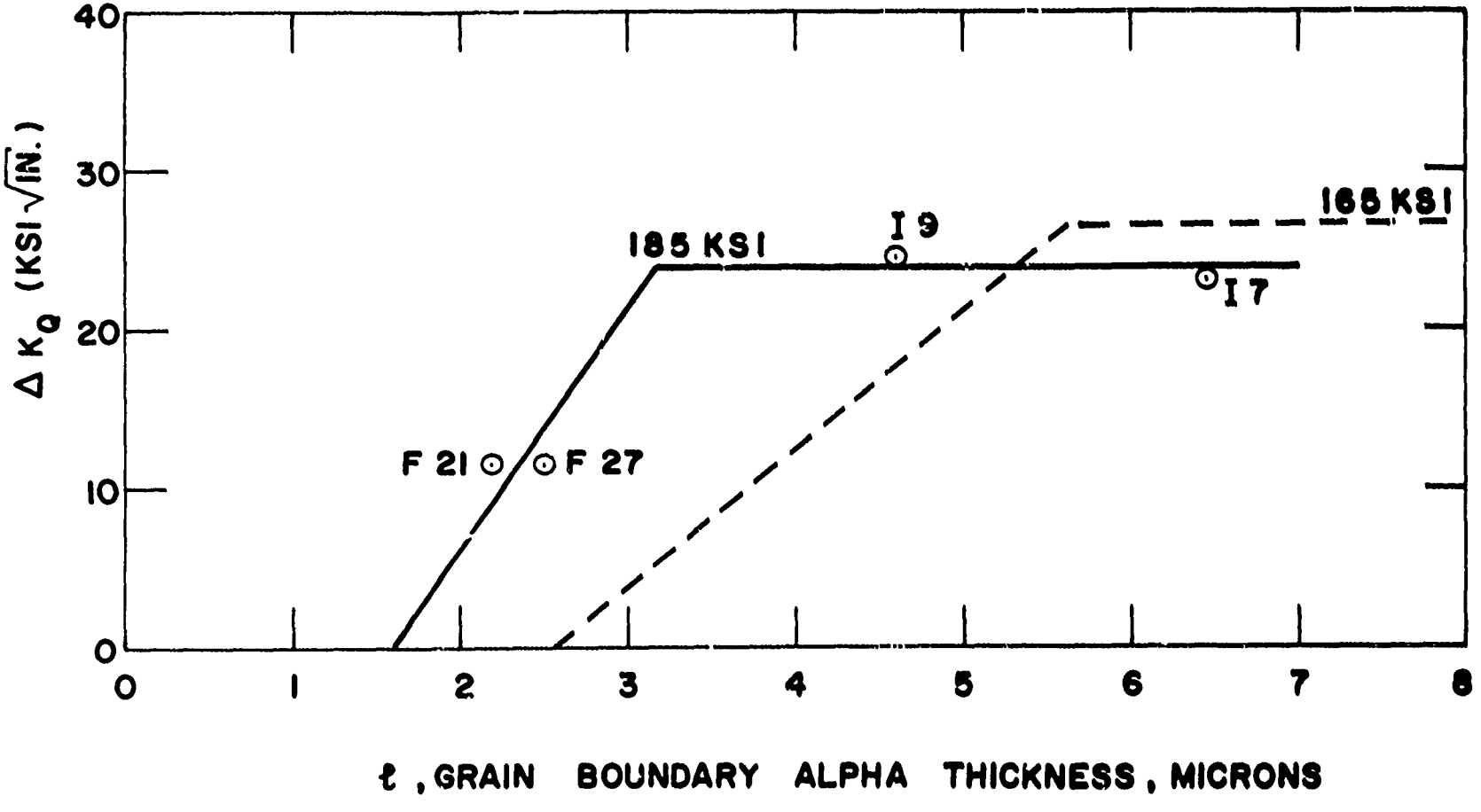

Figure 3. ΔK_Q vs Grain Boundary Alpha Thickness.

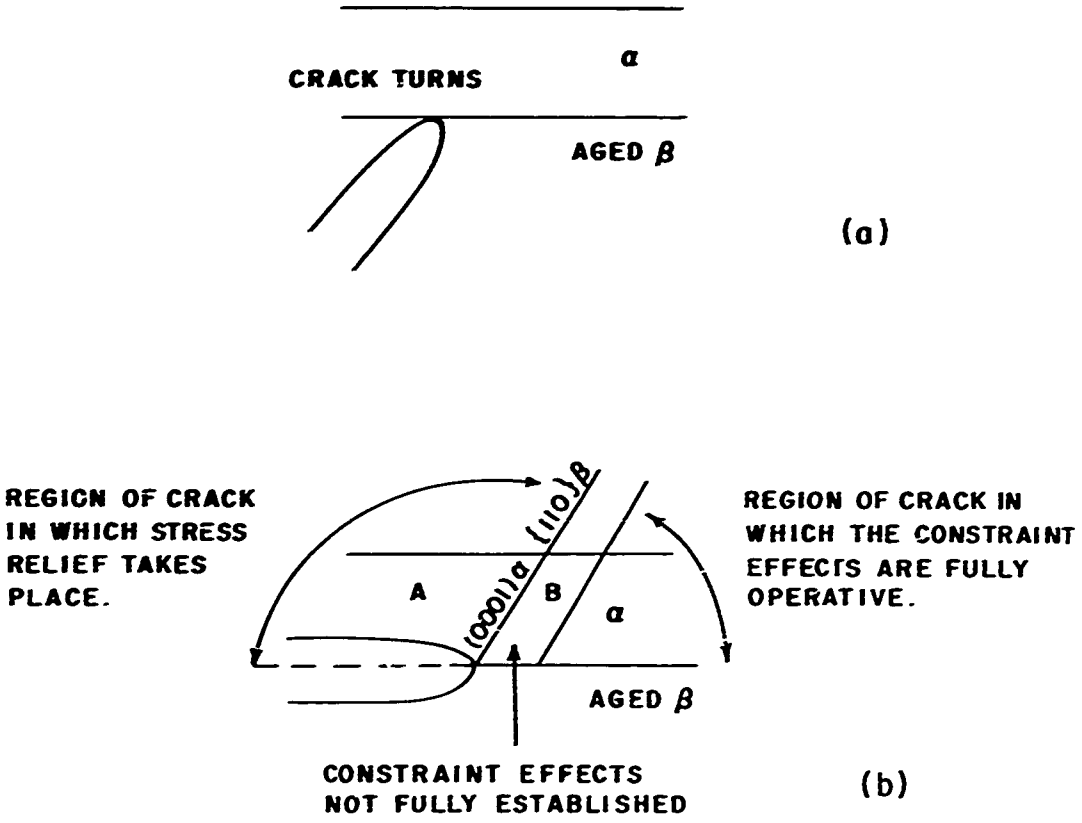

Figure 4. Crack at Grain Boundary Alpha Interface

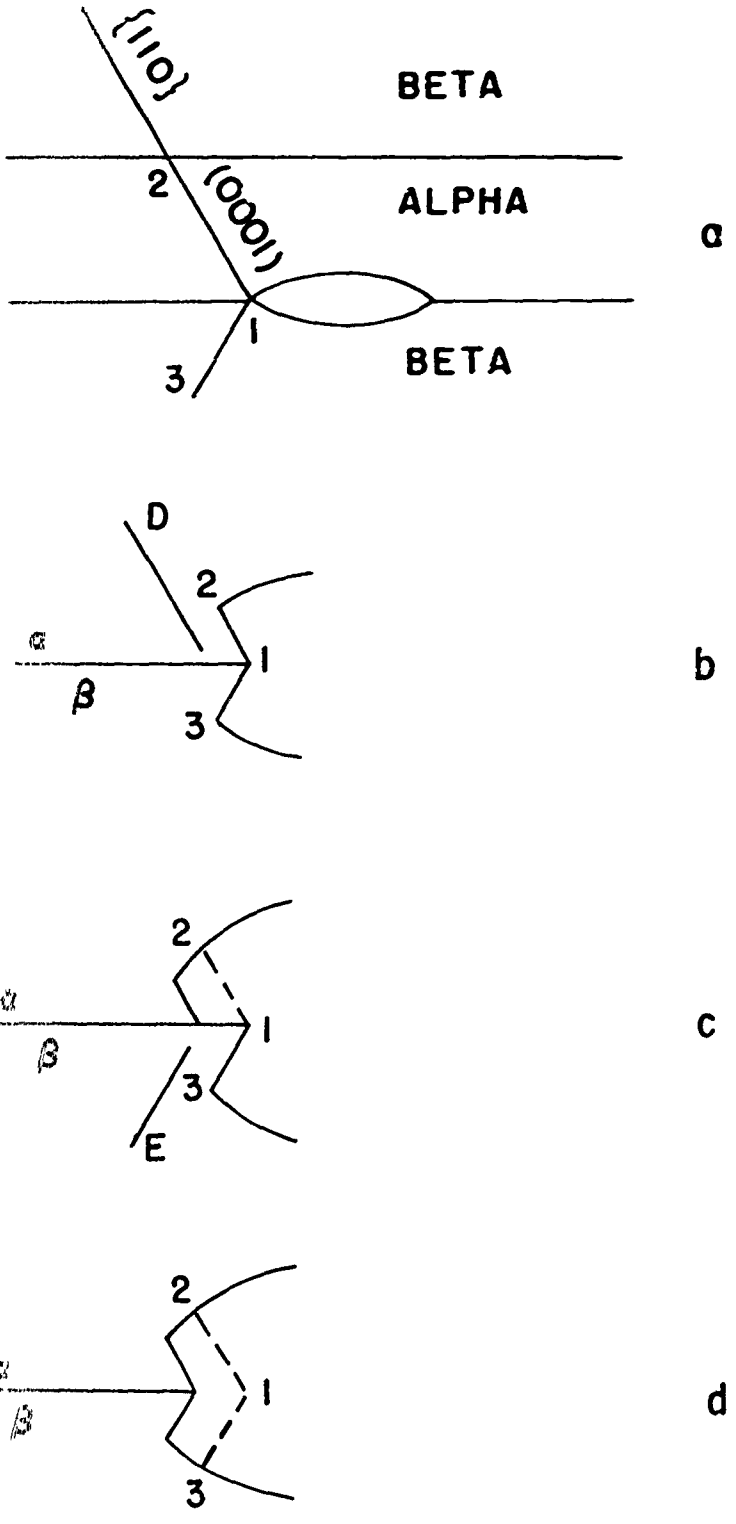

Figure 5. Flow at a Crack Tip.

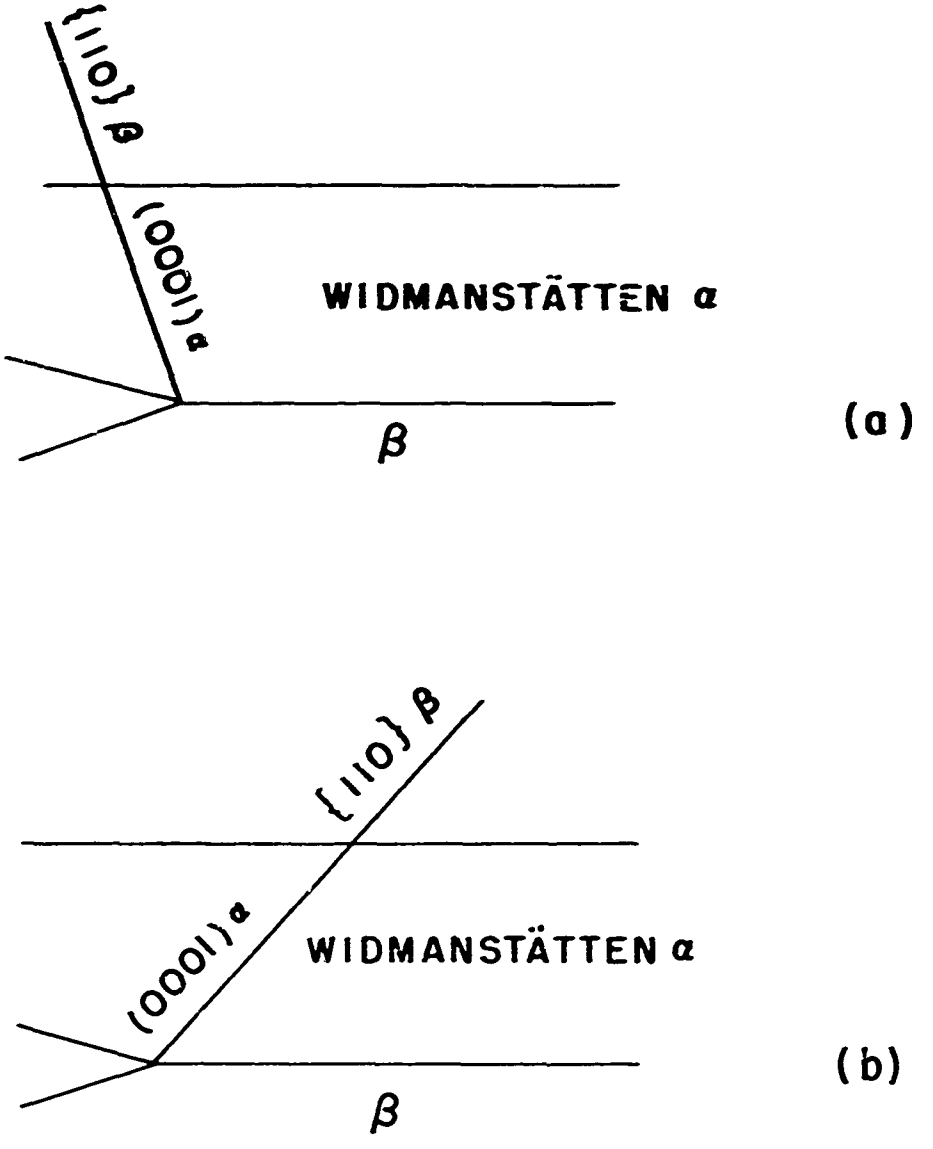

Figure 6. Crack at a Widmanstätten Alpha Plate.

Figure 7. Alpha Precipitation During Warm Working. X920.

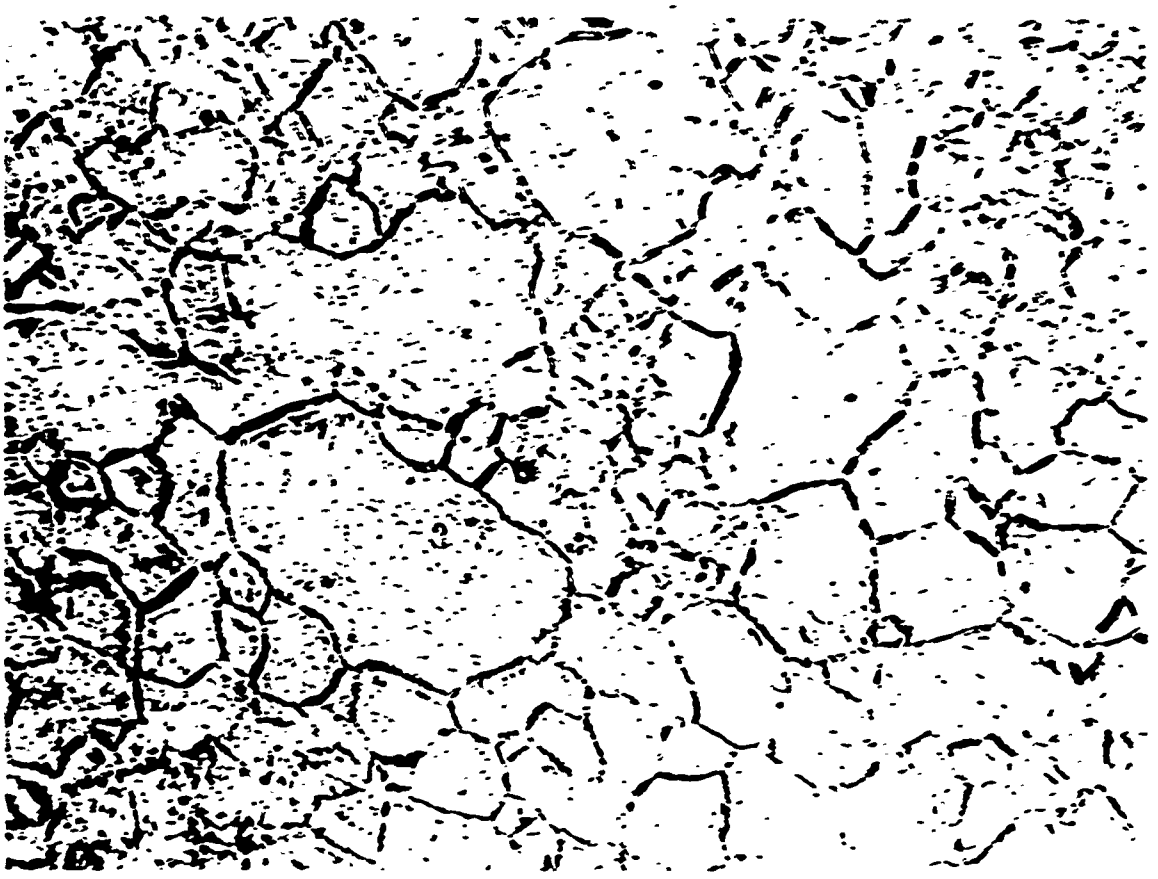

Figure 8. Bi-Modal Grain Size Found After Heat Treating Above the Beta Transus.

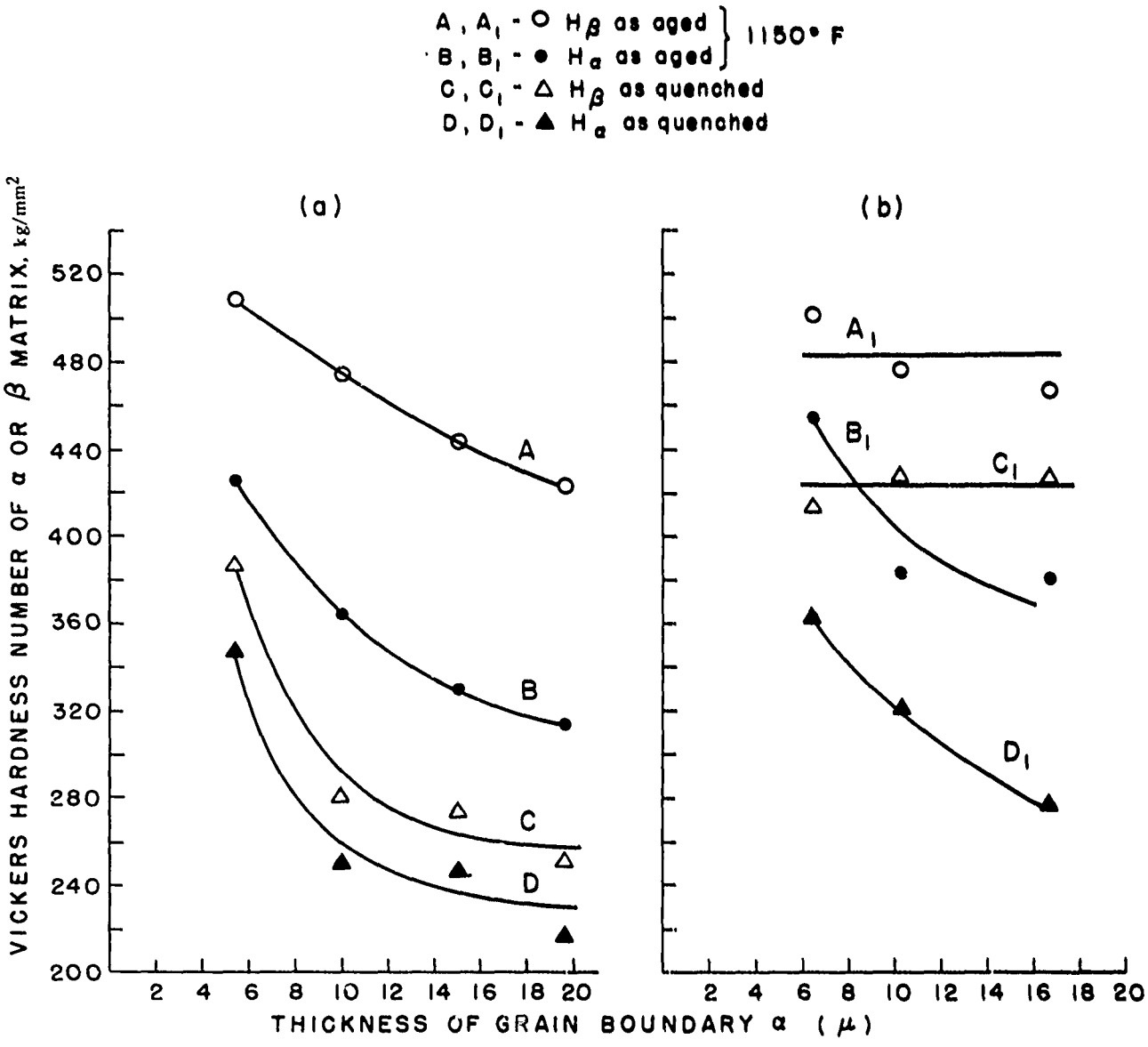

Figure 9. VHN vs Thickness of Grain Boundary Alpha.

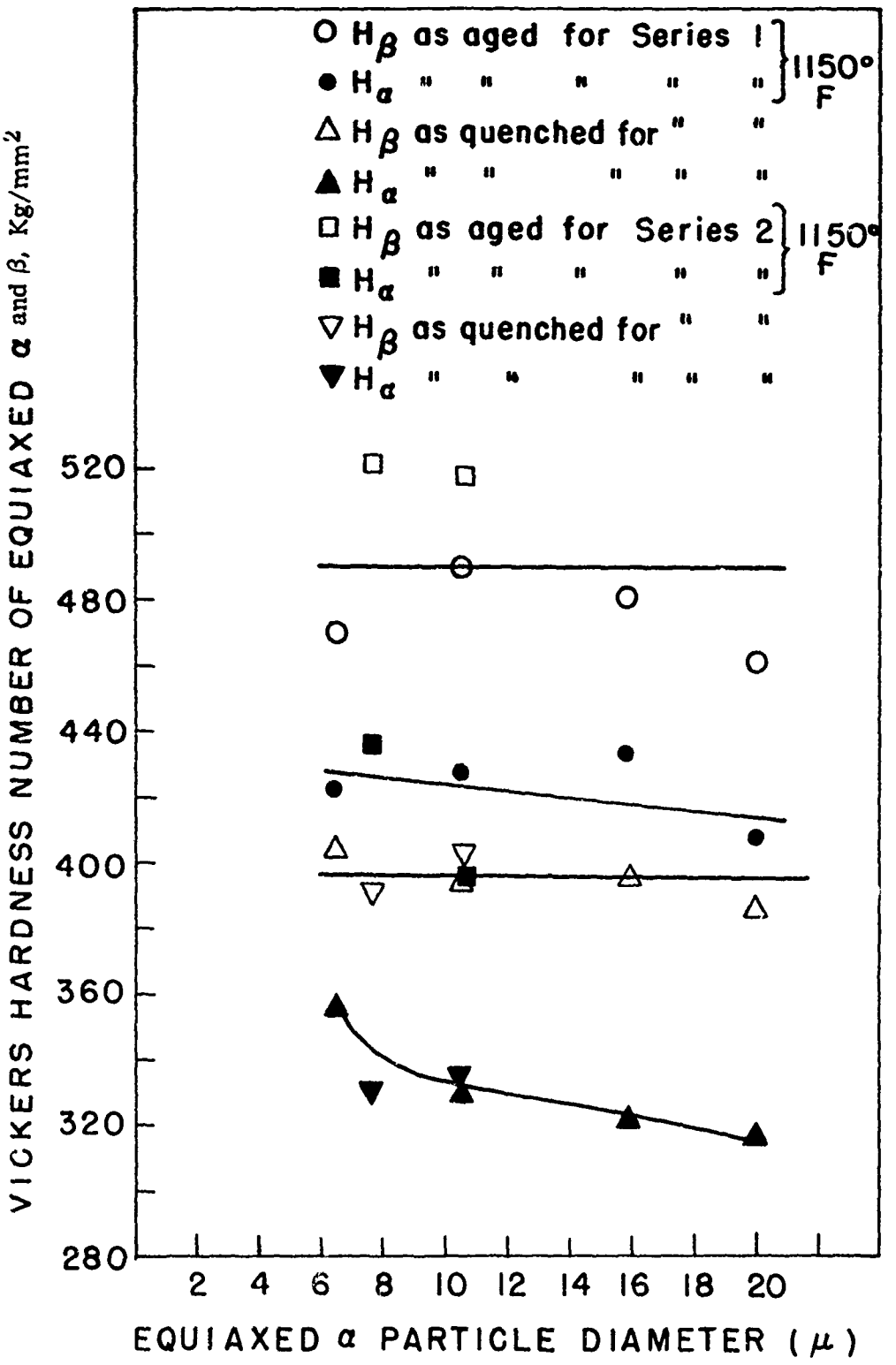

Figure 10. VHN vs Equiaxed Alpha Particle Size.

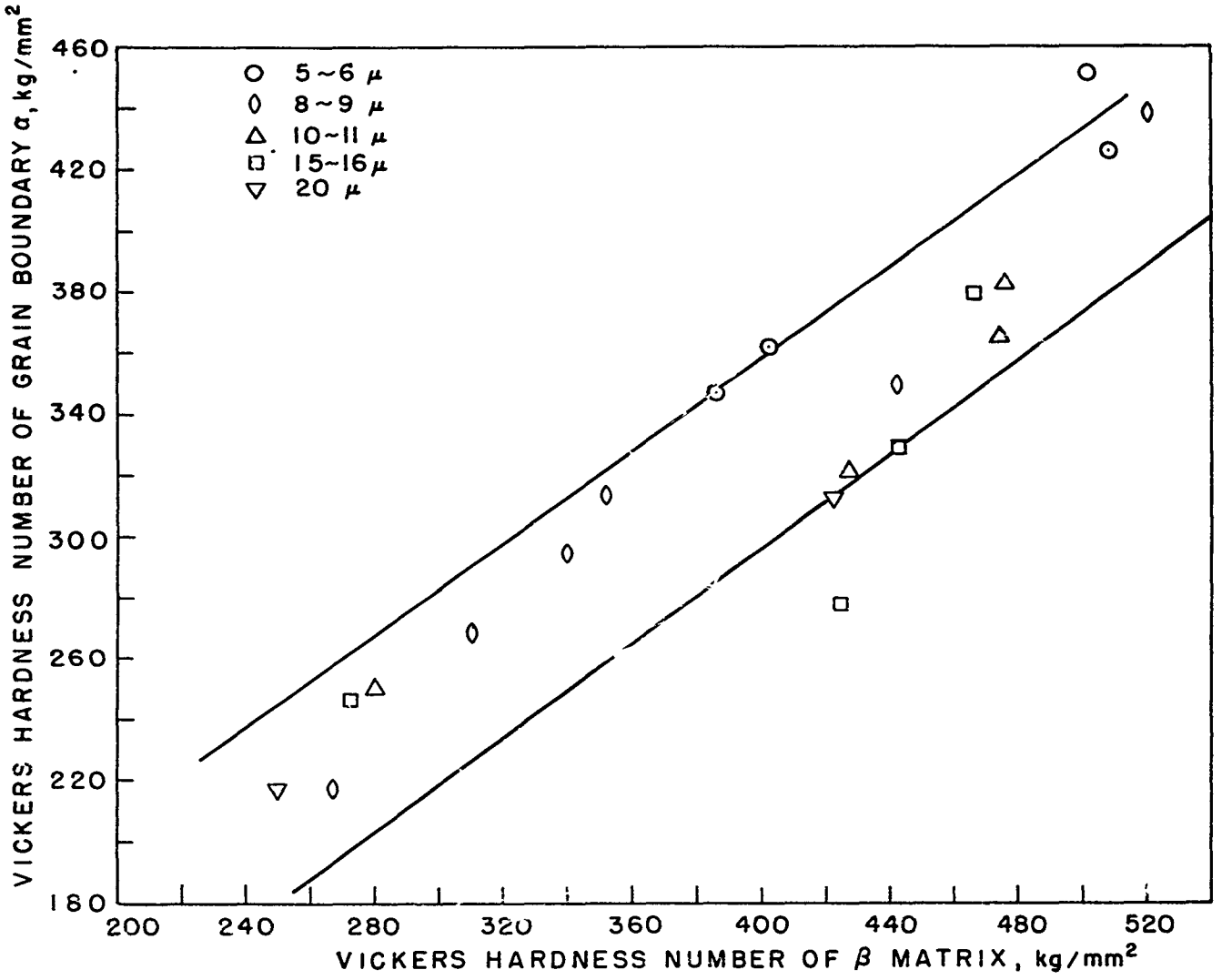

Figure 11. VHN of Grain Boundary Alpha vs VHN of β Matrix.

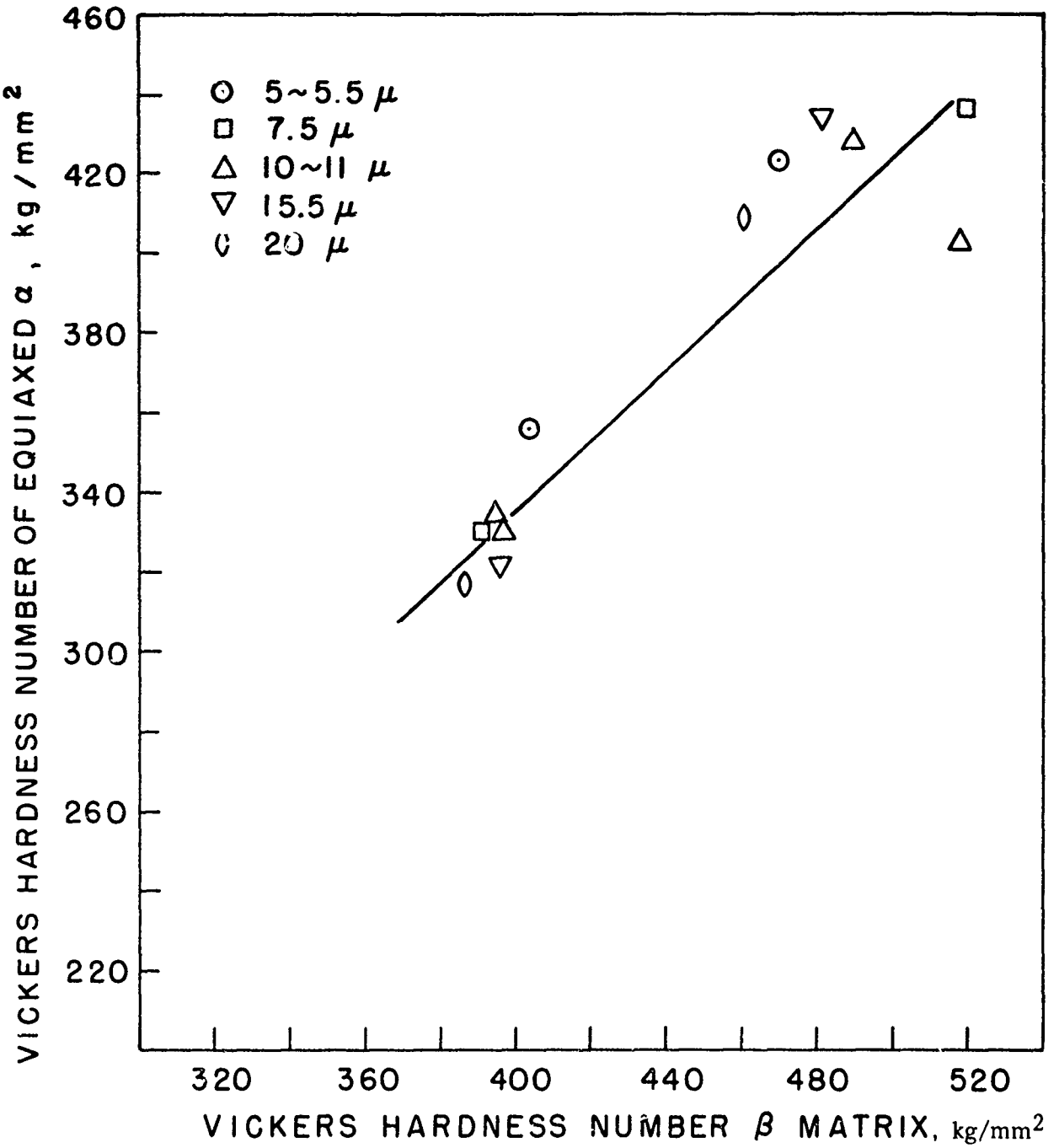

Figure 12. VHN of Equiaxed Alpha vs VHN of β Matrix.

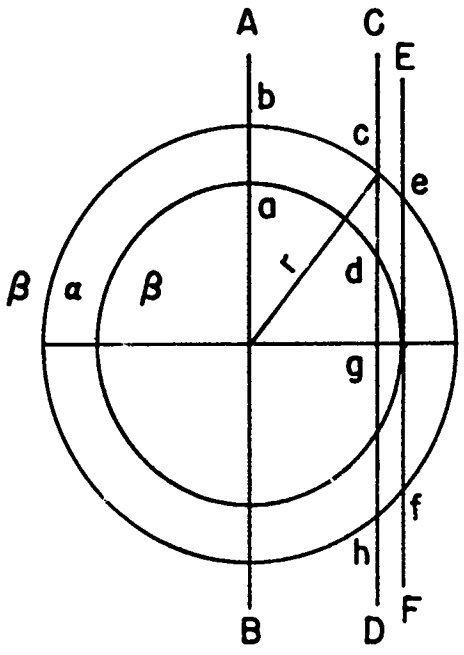

CD IS THE AVERAGE POSITION OF A LINE PASSED RANDOMLY THROUGH A SPHERE.

Figure 13. Geometrical Treatment of Grain Boundary Alpha Thickness.

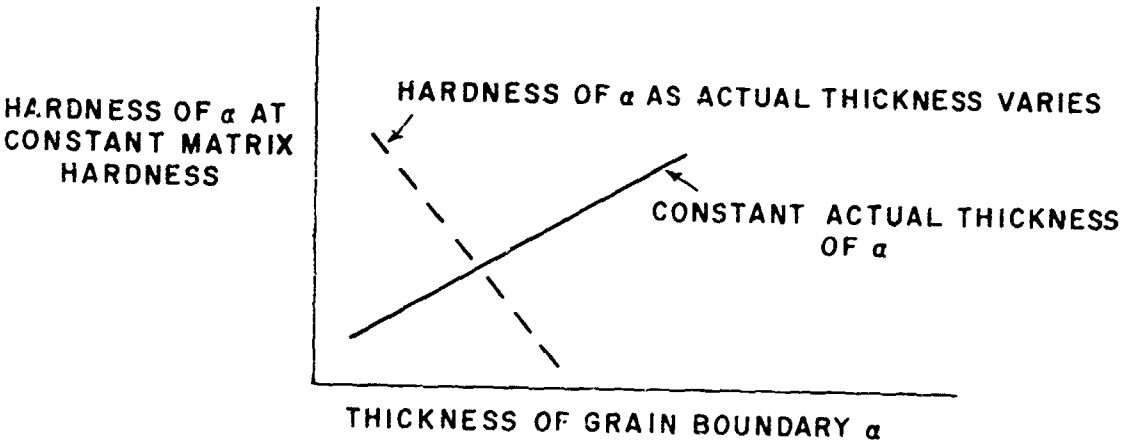

Figure 14. Variation in Hardness with Apparent Alpha Thickness.

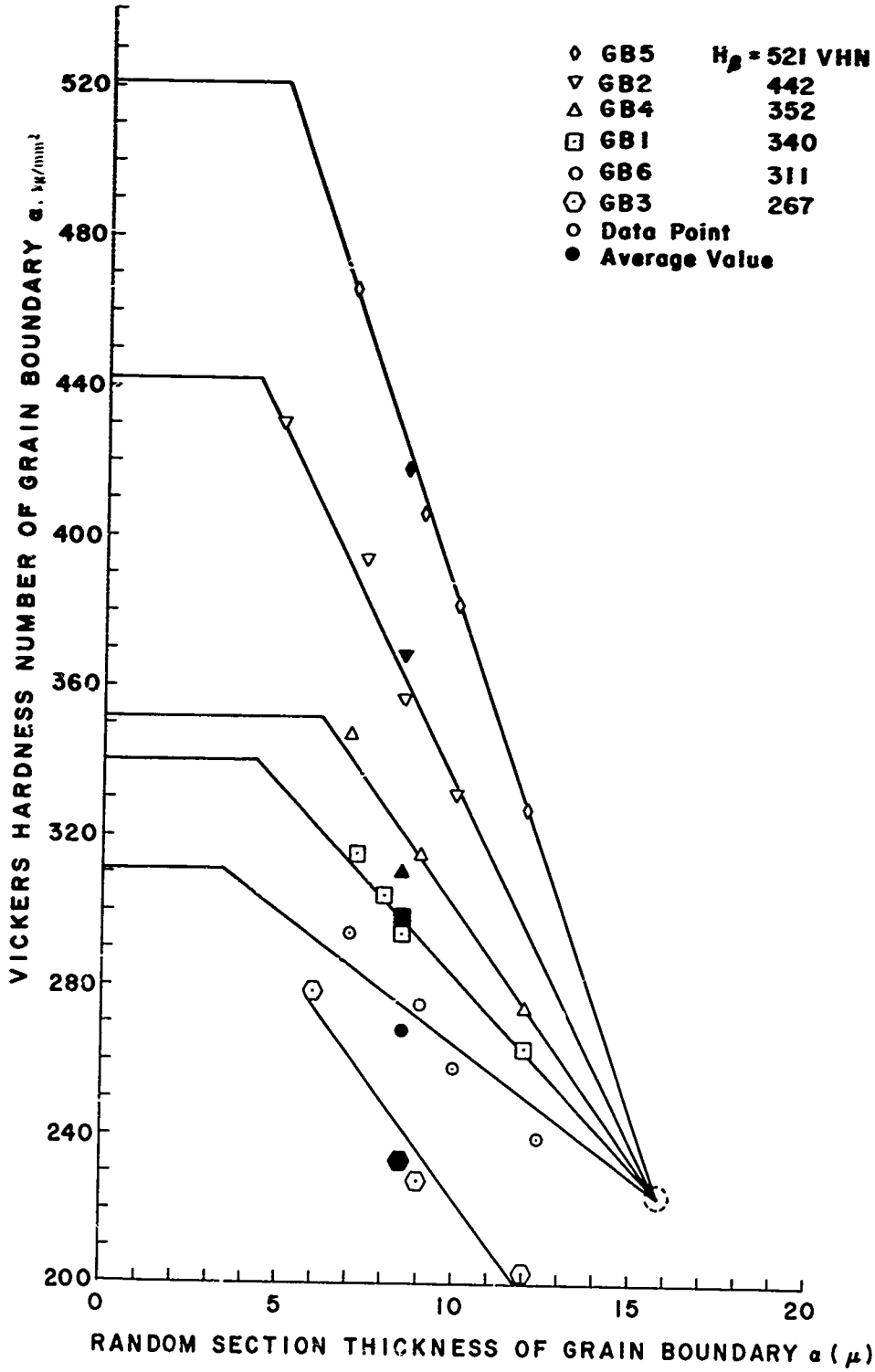

Figure 15. VHN of Alpha Versus Average Alpha Thickness at Constant Matrix Hardness.

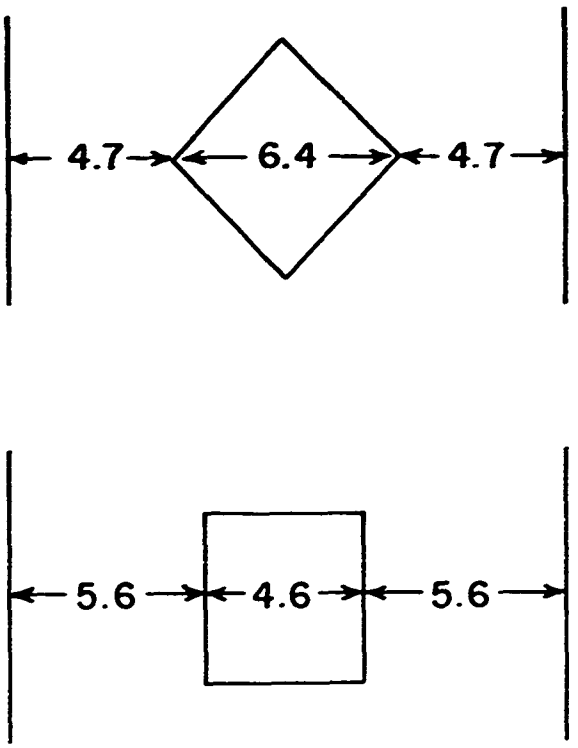

Figure 16. Diagram of Hardness Indentation.

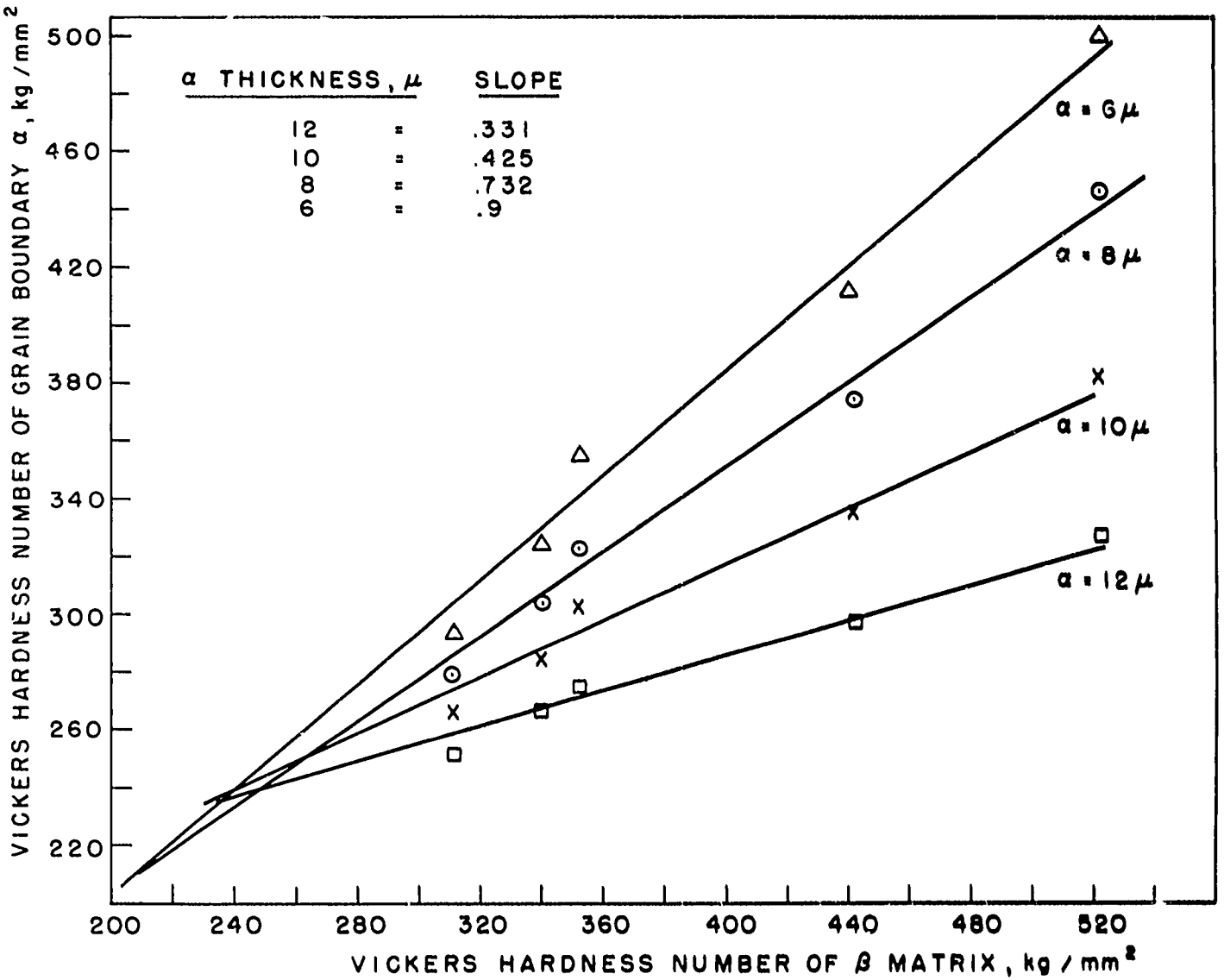

Figure 17. VHN of Grain Boundary Alpha vs Vickers Hardness Number of β Matrix.

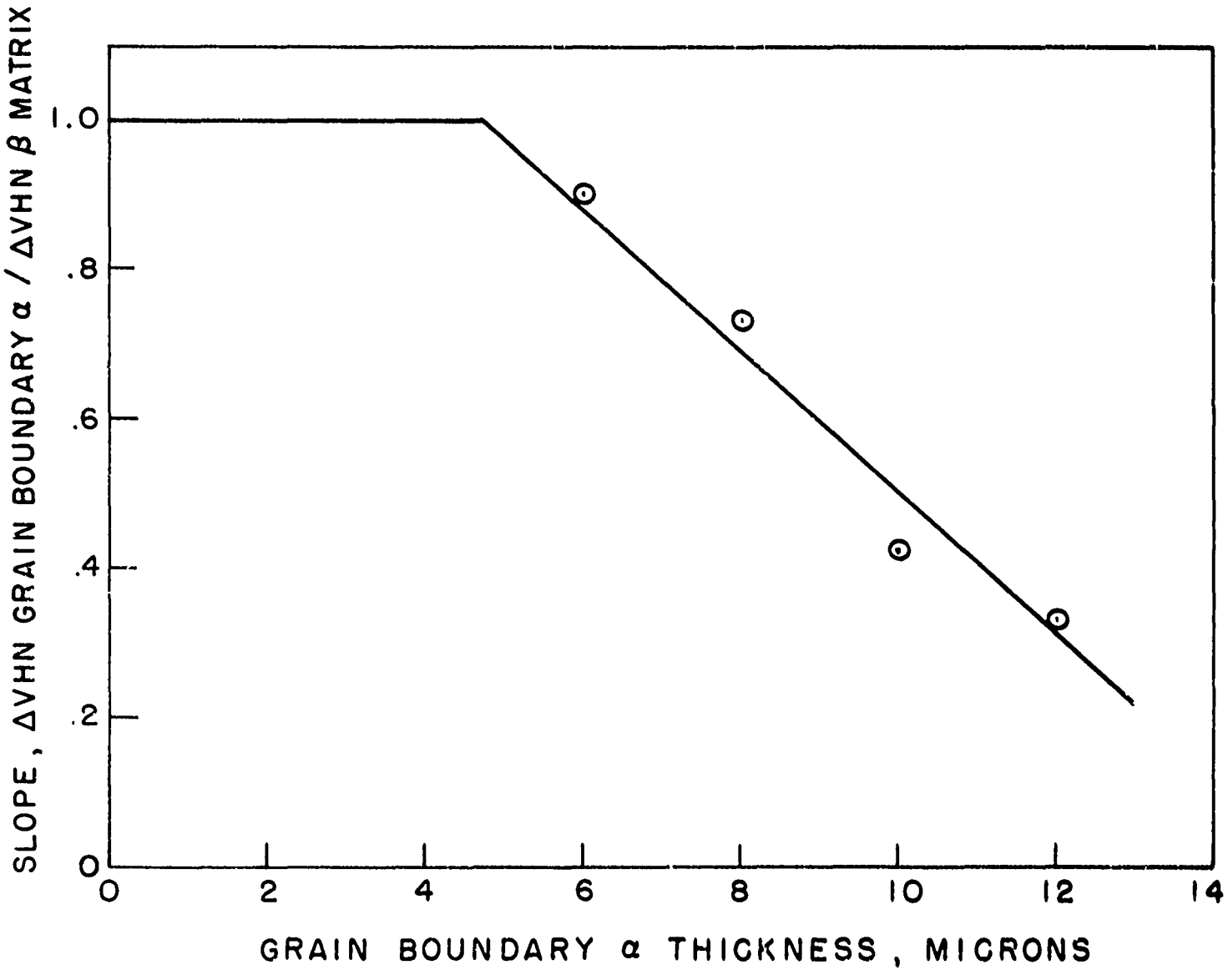

Figure 18. Slope, $\Delta VHN_{\alpha} / \Delta VHN_{\beta}$ vs Grain Boundary Alpha Thickness.

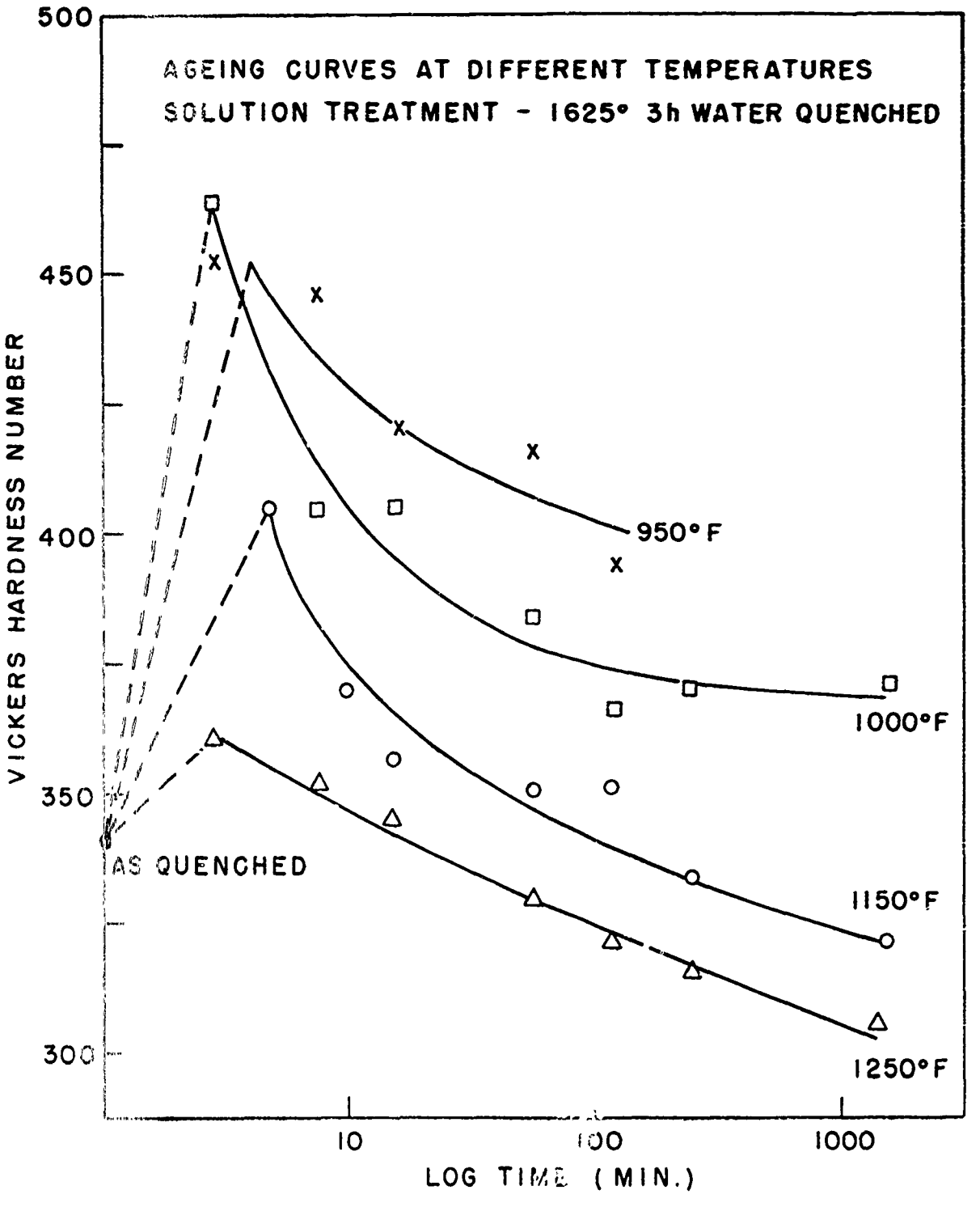

Figure 19. Age Hardening Behavior of Alloy #2

Figure 20. Selected Area Diffraction Pattern of Three Overlapping α' Axes Labeled A, B, and D.

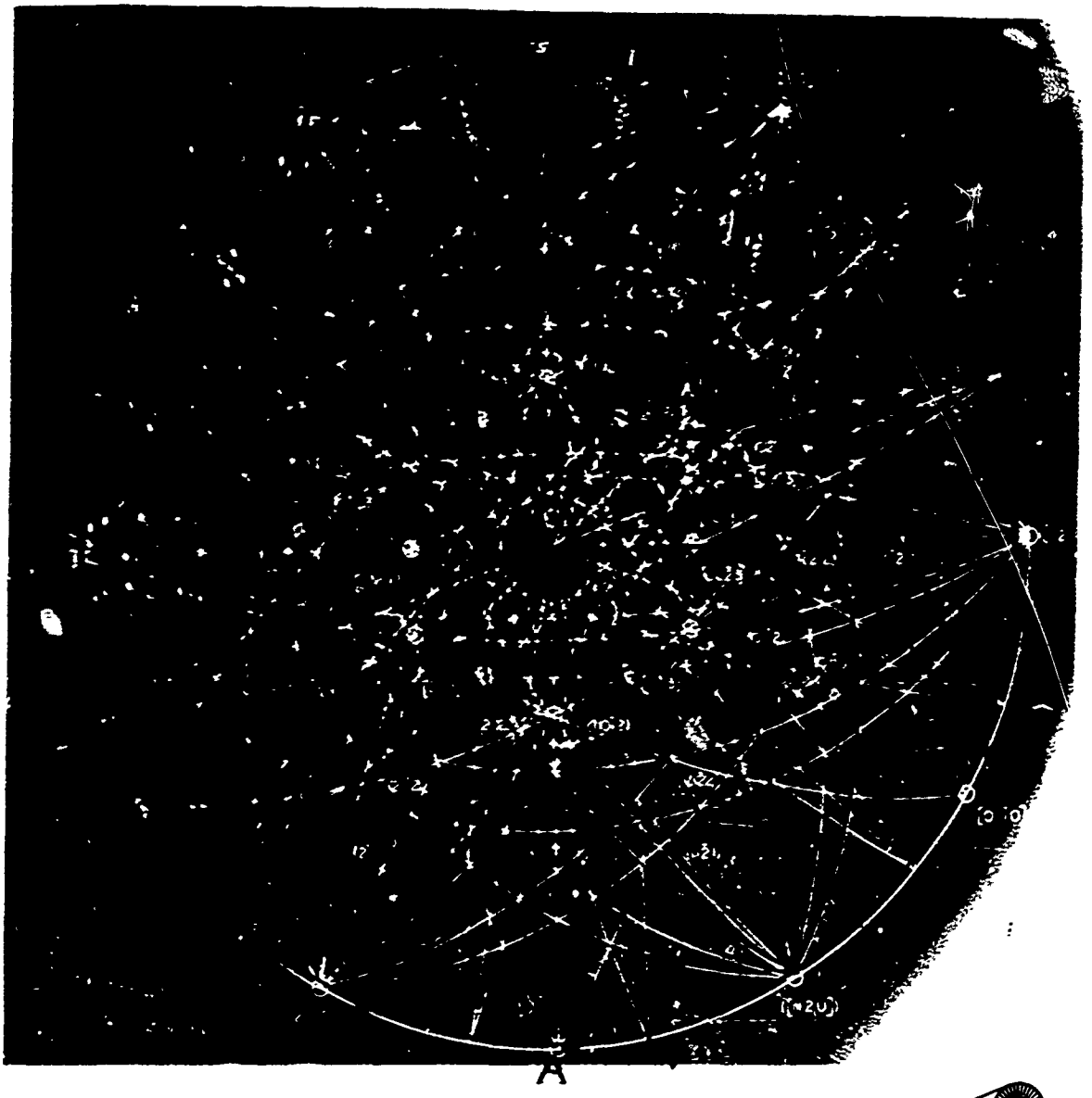

Figure 21. An Overlaid Transparent Stereographic Projection with the Zone Axes A, B, C, and D Indicated.

Figure 22a. A Beta Subgrain Enclosed by Several Equiaxed α Particles.

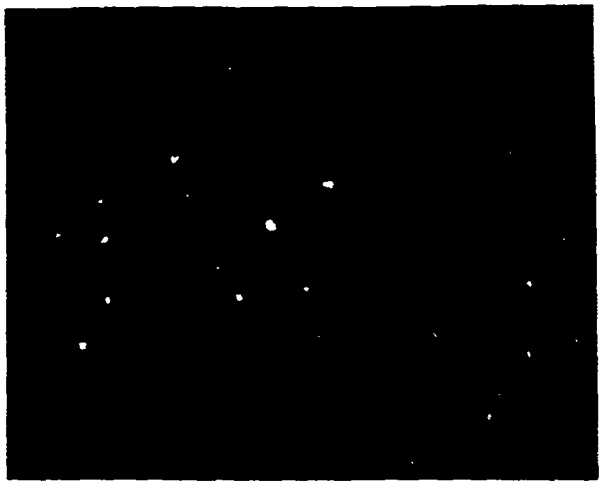

Figure 22b. Selected Area Diffraction Pattern Showing a Burgers Relationship Between an Equiaxed α Particle and the Beta Subgrain.

Figure 23. Alpha Bridge Connecting Two Equiaxed Alpha Particles.

Figure 24. Enlarged Region of Figure 23 Showing α Bridge.

Figure 25. Bright Field Micrograph of a Beta Subgrain.

Figure 26. Dark Field Micrograph of Lightning Bolt Type Martensite.

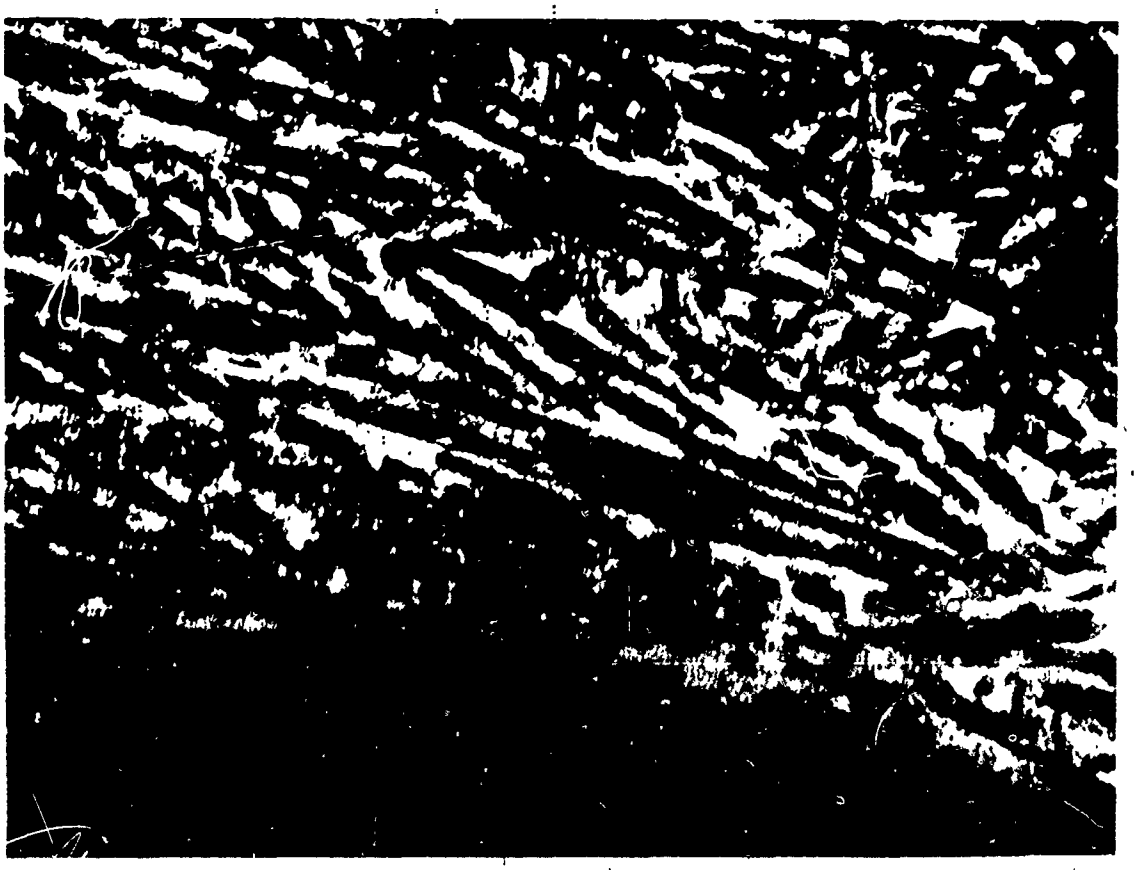

Figure 27a. Dark Field Micrograph Taken on a 112β Reflection Showing Small Martensite Plates.

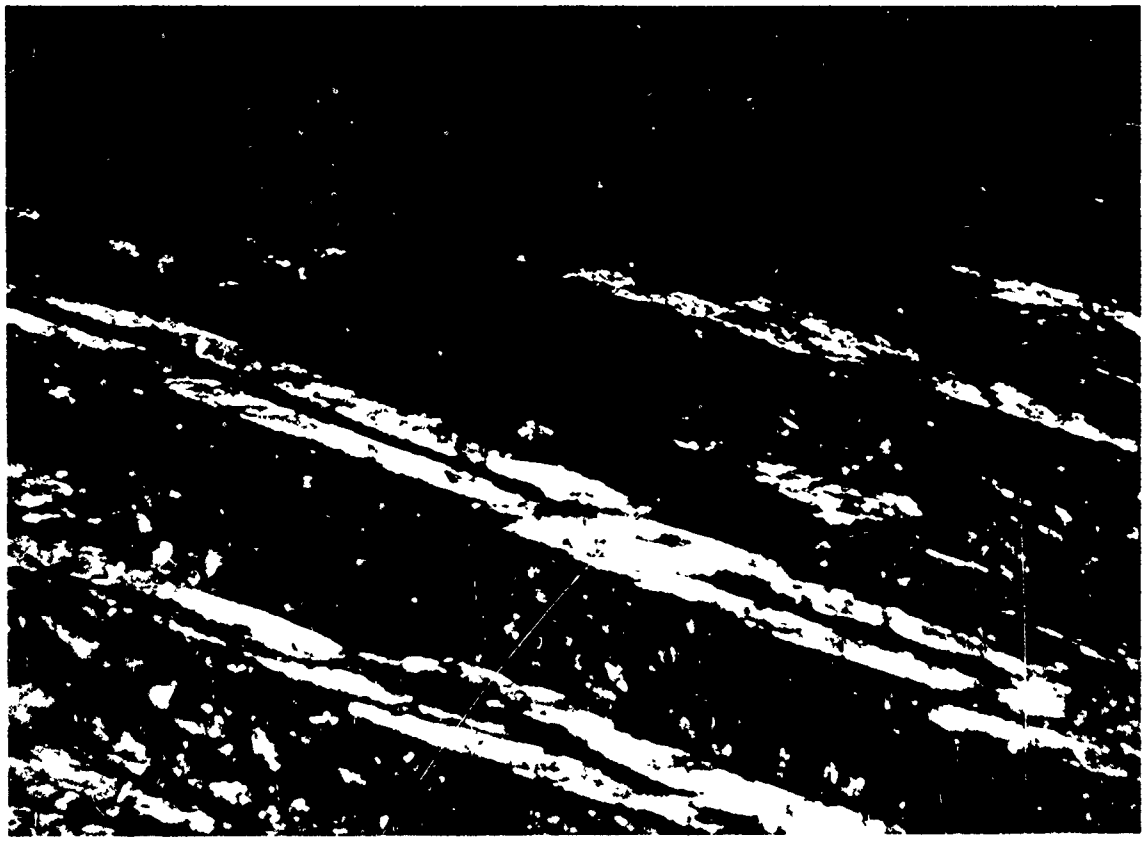

Figure 27b. Dark Field Micrograph Taken on an α' Reflection Showing Larger Martensite Plates.